Figure 4 Functional deficits in the HCN1 channel facilitate Aβ generation. (A) Quantification of endogenous murine Aβ40 and Aβ42 in the cortex of 4-month-old HCN1$^{+/+}$, HCN1$^{+/-}$, and HCN1$^{-/-}$ mice by using the sELISA system (left panels). Statistical analysis was performed using the two-tailed Mann–Whitney *U*-test (average ± SEM, n = 5, **p < 0.01). (B) Quantification of Aβ40 and Aβ42 secreted into the culture medium by N2a cells by using the sELISA system. FLAG-APP or FLAG-APP and HCN1 were transiently overexpressed in the cells with (+) or without (−) 10 μM ZD7288 (left panels). Statistical analysis was performed using one-way analysis of variance followed by Tukey's multiple comparison test (average ± SEM, n = 4, ***p < 0.001). Expression levels of APP and HCN1 was confirmed by immunoblotting (right panels in *A* and *B*).

selective inhibitor of HCN channel activity (compare lanes 3 through 6). Although we have not confirmed the blockage of channel activity electrophysiologically, ZD7288 had no effect on Aβ levels in cells without HCN1 expression (column 5), and APP expression was not affected by either the presence of HCN1 or by the administration of ZD7288 (Figure 4B, right panel). Furthermore, administration of ZD7288 did not influence the interaction of HCN1 with APP (Additional file 1: Figure S5). These results suggest that the suppression of Aβ generation in HCN1-overexpressing cells probably depends on channel activity (Figure 4B), in agreement with the *in vivo* observation that the brains of mice lacking the HCN1 gene and with impaired HCN channel activity (Figure 3B, D, and G) demonstrated increased Aβ generation (Figure 4A).

Association of HCN1 with APP *in vivo* and *in vitro*

Increased synaptic activity enhances Aβ generation [8-10], and modulation of Aβ generation is not limited to

alterations in HCN1 channel activity. Indeed, APP metabolism is thought to be largely regulated by APP-binding partners [14]. Therefore, we next explored the hypothesis that HCN1 might be involved in regulating APP metabolism via a physical interaction between the channel and APP. In support of this hypothesis, an anti-HCN1 antibody co-immunoprecipitated APP together with HCN1 from a lysate of wild type murine cortex (Figure 5A). The interaction seemed to be specific in that APP was not recovered from the cortical lysate of HCN1$^{-/-}$ mice. The association between APP and HCN1 was next confirmed in the EC. Using EC-rich brain samples isolated from HCN1$^{+/+}$ and HCN1$^{-/-}$ mice (Additional file 1: Figure S3A), a co-immunoprecipitation assay was performed with an anti-HCN1 antibody, and the immunoprecipitates were analyzed with the indicated antibodies (Figure 5B). Along with X11 and X11L, APP was co-immunoprecipitated with HCN1 in EC-rich brain samples of wild type mice (Figure 5B), suggesting that HCN1 can complex with

APP and X11/X11L *in vivo*. These results are in agreement with the co-localization results of HCN1, X11, and X11L in the wild type cortex shown above (Figure 3H–K). Tubulin and PSD95 (postsynaptic density protein 95) were not detected in the immunocomplex, indicating

the specific association of APP and X11/X11L with HCN1.

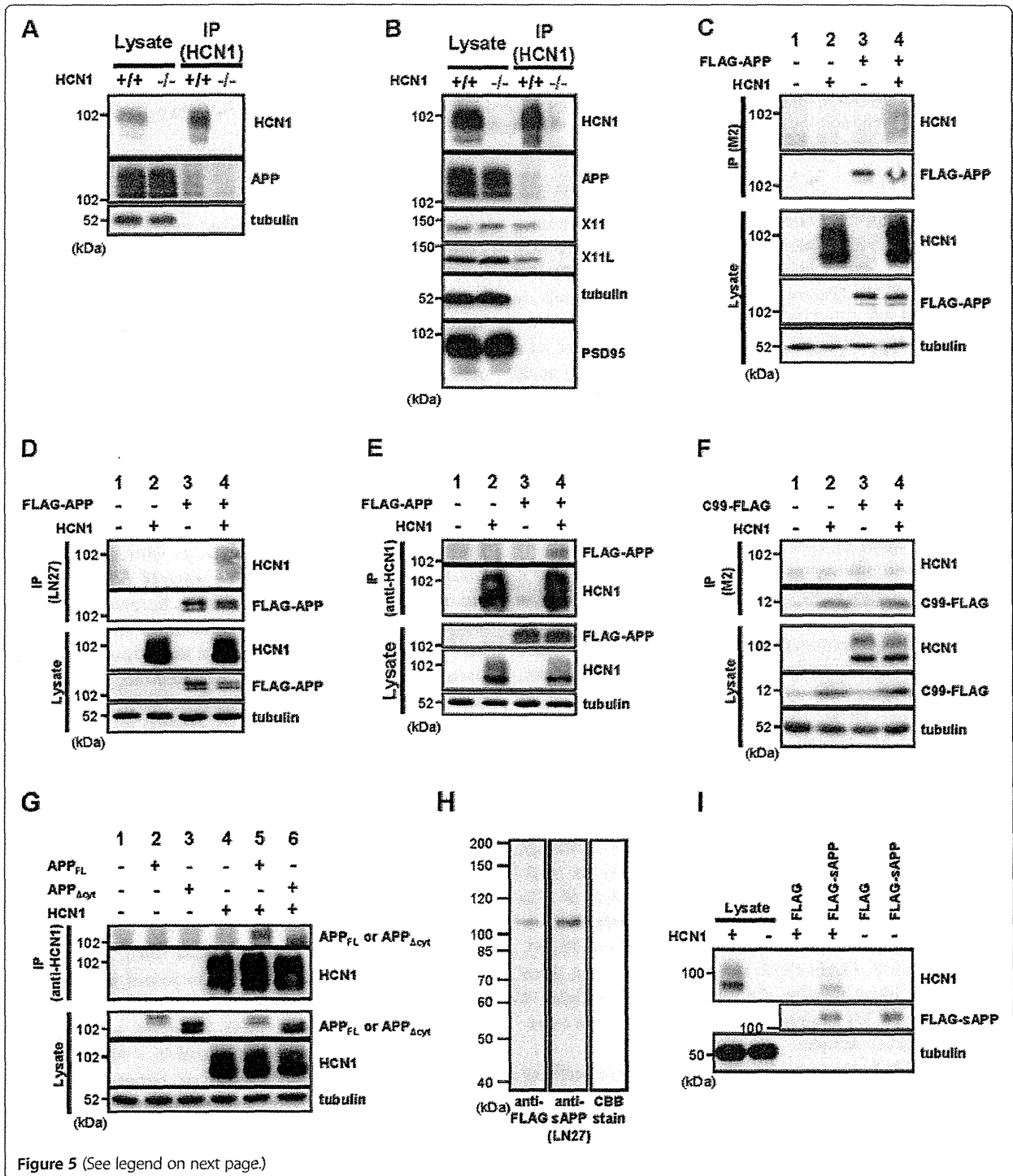To show whether HCN1 directly binds to APP without mediation by X11/X11L, FLAG-APP and HCN1 were transiently expressed in N2a cells and a co-immunoprecipitation

Figure 5 (See legend on next page.)

(See figure on previous page.)
Figure 5 APP and HCN1 form a molecular complex *in vivo* and *in vitro*. (**A**) Co-immunoprecipitation of the HCN1-APP complex from the wild type and HCN1$^{-/-}$murine cortex. Brain lysates were immunoprecipitated with an anti-HCN1 antibody. Immunocomplexes were detected by immunoblotting. (**B**) Co-immunoprecipitation of HCN1-APP, -X11 and -X11L complexes from the EC-rich cortex (see Additional file 1: Figure S2). Brain lysates were immunoprecipitated with an anti-HCN1 antibody. Immunocomplexes were detected by immunoblotting. (**C-G**) Co-immunoprecipitation of the HCN1-APP complex from N2a cells transiently overexpressing FLAG-APP and murine HCN1. (**C-E**), Analysis of FLAG-APP and murine HCN1, (**F**) C99-FLAG and murine HCN1, and (**G**) APP$_{FL}$ or APP$_{\Delta cyt}$ and murine HCN1 immunocomplexes. To standardize the amount of plasmid, empty vector (−) was added to yield 1.2 μg of plasmid in total. Cell lysates were immunoprecipitated with anti-FLAG M2 (**C** and **F**), anti-APP extracellular domain (LN27) (**D**), or anti-HCN1 (**E** and **G**) antibodies. Immunocomplexes were detected by immunoblotting. (**H**) Affinity purification of FLAG-sAPP secreted into the culture medium by N2a cells expressing FLAG-APP. The purification was performed using anti-FLAG M2 affinity beads. FLAG-sAPP were specifically detected by M2 and anti-APP extracellular domain (LN27) antibodies, and no contaminating bands were identified by CBB-staining. (**I**) Pull-down of HCN1 with affinity purified FLAG-sAPP prepared in (H). Lysates from wild type cells (−) and cells that transiently expressed HCN1 (+) were incubated with M2 affinity beads coupled with FLAG-tag or FLAG-sAPP. The complexes resulting from the pull-down assay were subjected to immunoblot analysis with anti-HCN1 antibody.

assay was performed. The anti-FLAG M2 antibody immunoprecipitated HCN1 along with FLAG-APP (Figure 5C). An anti-hAPP extracellular domain antibody (LN27) also recovered HCN1 (Figure 5D), and anti-HCN1 antibody recovered FLAG-APP (Figure 5E).

APP is a type I transmembrane protein composed of a large extracellular (luminal) domain of 596 amino acids and a small intracellular domain of 47 amino acids. On the other hand, HCN1 is six-transmembrane protein with short extracellular sequences between transmembrane regions one and two, three and four, and five and six; and long intracellular domains within the amino- and carboxyl-terminal regions of the protein. To determine the region of APP that binds to HCN1, we performed co-immunoprecipitation assays using APP deletion mutants (C99-FLAG, which largely lacks the extracellular domain of APP and in which FLAG is fused to the carboxyl terminal region of APP; and APP$_{\Delta cyt}$, which lacks the 43- amino acid carboxyl terminal region of APP) (Figure 5F, G). The results of this assay indicated that HCN1 was not co-immunoprecipitated with C99-FLAG (Figure 5F), whereas APP$_{\Delta cyt}$ was co-immunoprecipitated with HCN1 (Figure 5G).

Next, we performed an *in vitro* pull-down assay with FLAG-soluble APP (FLAG-sAPP, consisting of the extracellular domain of APP cleaved at the α- and/or β-cleavage sites). FLAG-sAPP was purified with affinity beads (anti-FLAG M2 affinity gel) from the culture medium of N2a cells expressing FLAG-APP (Figure 5H) and then incubated with lysates of N2a cells that expressed HCN1. HCN1 bound to FLAG-sAPP, but not to FLAG-tag alone (Figure 5I). Taken together, the results shown in Figure 5 indicate that HCN1 associates with APP through its extracellular (luminal) domain.

Hence, HCN1 apparently interacts with the extracellular domain of APP (Figure 5) and with both X11 and X11L in the cytoplasm (Figure 3H–K, Figure 5B). This suggests that the HCN1 channel might form a ternary complex with APP and either X11 or X11L to regulate Aβ

generation. However, the detailed molecular regulation of complex formation remains to be determined.

Age- and AD state-dependent HCN disruption in the temporal cortex (superior temporal gyrus) of cynomolgus monkeys and sporadic AD patients

Advanced age is the greatest risk factor for AD. To examine the relationship between aging and HCN1 levels, we quantified the amount of HCN1, Aβ, APP, and actin in freshly frozen brain tissues (superior temporal gyrus) from cynomolgus monkeys of various ages (Figure 6A and Additional file 1: Figure S6). Senile plaques and neurofibrillary tangles spontaneously appear in the brains of cynomolgus monkeys with advancing age [32,33], and the amino acid sequence of Aβ in cynomolgus monkeys is identical to that in humans [34]. Thus, we hypothesized that the cynomolgus monkey would be a useful animal model for the investigating the relationship between aging and AD pathology. Significant negative correlations were found between HCN1 levels and age (n = 39, r = −0.5363, p = 0.0004) (Figure 6A, left), between HCN1 and APP levels (n = 39, r = −0.3796, p = 0.0086) (Additional file 1: Figure S6B), between HCN1 and TBS-insoluble Aβ40 levels (n = 39, r = −0.2878, p = 0.0421) (Additional file 1: Figure S6C and D), and between HCN1 and Tris buffered saline (TBS)-insoluble Aβ42 levels (n = 39, r = −0.2913, p = 0.0401) (Additional file 1: Figure S6E and F). A significant positive correlation was found between age and APP level (n = 39, r = 0.8156, p < 0.0001) (Additional file 1: Figure S6A), and a significant weak-positive correlation was found between APP and TBS-insoluble Aβ42 levels (n = 39, r = 0.3714, p = 0.0236) (Additional file 1: Figure S6H). However, no correlation was found between age and actin level (n = 39, r = −0.1981, p = 0.2266) (Figure 6A, right) or between APP and TBS-insoluble Aβ40 levels (n = 39, r = 0.2993, p = 0.072) (Additional file 1: Figure S6G).

Finally, we examined the possibility of altered HCN1 levels in human AD brain specimens obtained at autopsy
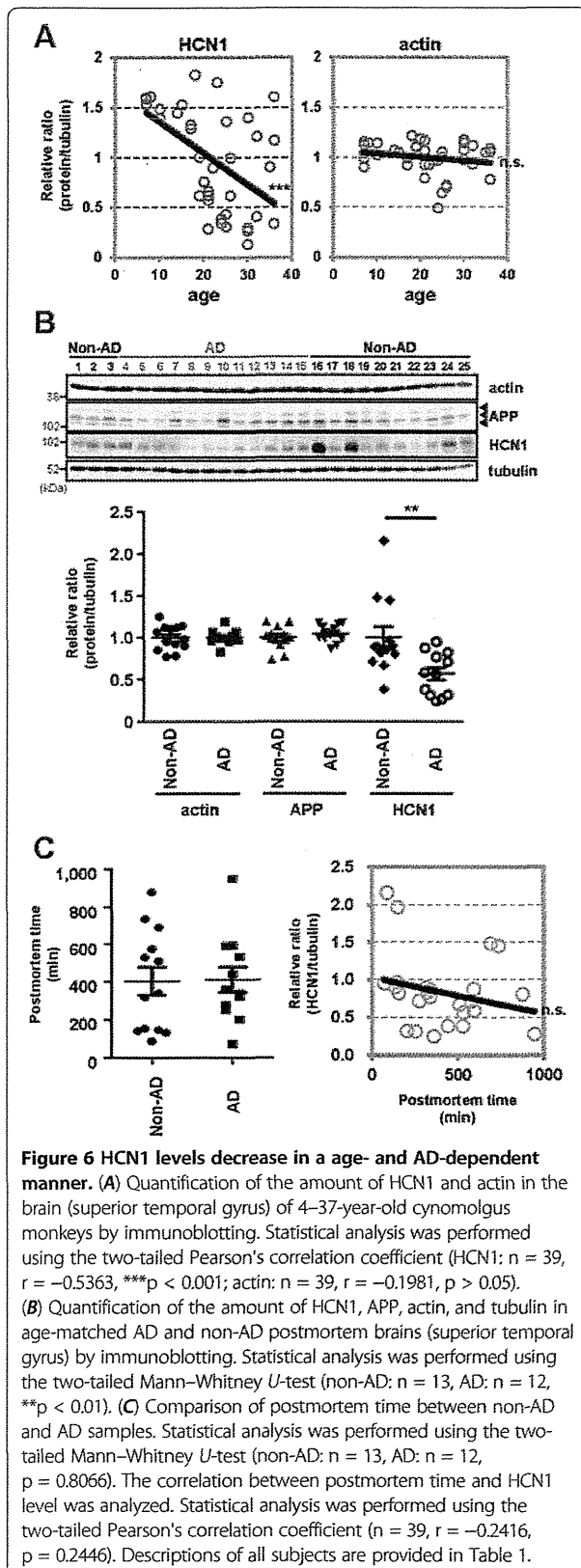
Figure 6 HCN1 levels decrease in a age- and AD-dependent manner. (A) Quantification of the amount of HCN1 and actin in the brain (superior temporal gyrus) of 4–37-year-old cynomolgus monkeys by immunoblotting. Statistical analysis was performed using the two-tailed Pearson's correlation coefficient (HCN1: n = 39, r = −0.5363, ***p < 0.001; actin: n = 39, r = −0.1981, p > 0.05).
(B) Quantification of the amount of HCN1, APP, actin, and tubulin in age-matched AD and non-AD postmortem brains (superior temporal gyrus) by immunoblotting. Statistical analysis was performed using the two-tailed Mann–Whitney U-test (non-AD: n = 13, AD: n = 12, **p < 0.01). (C) Comparison of postmortem time between non-AD and AD samples. Statistical analysis was performed using the two-tailed Mann–Whitney U-test (non-AD: n = 13, AD: n = 12, p = 0.8066). The correlation between postmortem time and HCN1 level was analyzed. Statistical analysis was performed using the two-tailed Pearson's correlation coefficient (n = 39, r = −0.2416, p = 0.2446). Descriptions of all subjects are provided in Table 1.

(Figure 6B and Table 1). The postmortem time was not significantly different for the AD and non-AD brain samples used in this study (non-AD: n = 13, AD: n = 12, p = 0.8066), and no significant decrease in HCN1 levels related to postmortem time was observed (n = 25, r = −0.2416, p = 0.2446) (Figure 6C and Table 1). Of great relevance to this study, the amount of HCN1 was significantly reduced in AD brains (superior temporal gyrus) compared with that in age-matched control brains (non-AD: n = 13, AD: n = 12, p = 0.0083), while the levels of APP and actin were not significantly altered (Figure 6B and Table 1). These results suggest that the reduction in HCN1 expression that occurs with age (Figure 6A) may be involved in the aggravation of the pathology of AD.

Discussion

X11 and X11L are well-characterized neural adaptor proteins that regulate the trafficking and metabolism of APP [14]. Many reports indicate that X11s bind to APP and suppress Aβ generation *in vitro* and *in vivo* [14-22]. Furthermore, X11s are thought to mediate a number of cellular functions through their association with various proteins [35]. This report showed that mutant mice lacking both X11 and X11L present with dysfunctional HCN1 channel activity and epileptic seizures. Notably, AD patients are also at increased risk of epileptic seizures. Furthermore, mutant mice lacking HCN1 demonstrated increased generation of Aβ, which is a causative factor for the development of AD.

The incidence of AD dramatically increases with age. We found that the amount of HCN1 decreased with both aging and in AD. The dysfunction of HCN1 that occurs over time may, thus, be a trigger for epileptic seizures and the pathogenic generation of Aβ in AD.

Several converging studies corroborate the premise that HCN channel activity is closely related to epileptogenesis [11]. For example, HCN1 expression is significantly reduced in the EC after temporal lobe epilepsy [36,37]. Furthermore, HCN1 channel plasticity in cortical neurons is similar in multiple epileptic animal models [38-43]. Moreover, kainic acid-induced seizure susceptibility is increased in HCN1$^{-/-}$ mice [27], and HCN2-deficient mice exhibit spontaneous absence seizures [26].

HCN1$^{-/-}$ mice show a significantly higher number of negative resting membrane potentials and a significantly higher input resistance measured from responses to either negative or positive current steps [28]. As such, seizure susceptibility is increased in HCN1$^{-/-}$ mice [27], indicating that loss of the HCN1 subunit enhances neuronal excitability, which can increase Aβ generation [8-10]. These observations suggest that enhanced Aβ generation in HCN1$^{-/-}$ mice results from neuronal hyper-excitability, which is in turn caused by ablation of the HCN1 gene.

Table 1 Summary of subject information presented in Figure 6B and C

Sample no.	Subject	Age	Sex	Post mortem time (min)	Braak stage	Seizure	Relative ratio (protein/tubulin)		
							Actin	APP	HCN1
1	Normal	84	F	877	1	-	0.929	1.192	0.809
2	Normal	88	F	144	1	-	0.856	1.046	0.859
3	Normal	70	M	340	0.5	-	0.955	1.189	0.859
4	AD	84	M	71	4	-	0.950	1.171	0.952
5	AD	70	M	276	4	-	0.829	0.986	0.716
6	AD	74	M	322	5	-	0.961	0.990	0.827
7	AD	75	M	594	6	-	1.069	1.176	0.589
8	AD	76	M	947	6	+	1.190	1.167	0.273
9	AD	79	F	203	5	-	1.019	0.913	0.317
10	AD	81	M	360	6	-	0.971	0.862	0.247
11	AD	81	F	442	5	-	0.971	0.862	0.385
12	AD	82	F	254	6	-	0.988	1.029	0.313
13	AD	82	F	533	5	-	0.988	1.001	0.566
14	AD	82	F	338	4	-	1.028	1.063	0.770
15	AD	84	M	590	5	-	1.071	1.128	0.876
16	Normal	78	F	87	2	-	1.108	1.138	2.153
17	Normal	81	M	134	1	-	1.122	0.971	0.902
18	Normal	82	F	148	1	-	1.178	1.109	1.963
19	Normal	82	F	155	2	-	1.141	1.026	0.821
20	Normal	80	M	317	2	-	1.254	1.037	0.893
21	Normal	80	M	510	2	-	1.071	0.778	0.669
22	Normal	82	M	530	1	-	0.979	0.916	0.384
23	Normal	78	M	575	1	-	0.905	1.007	0.713
24	Normal	78	M	690	1	-	0.784	0.986	1.479
25	Normal	82	M	736	1	-	0.774	0.743	1.448

Postmortem brain samples were obtained from the Brain Bank for Aging Research, Tokyo Metropolitan Institute of Gerontology. Experimental procedures were approved by the appropriate ethical boards at each institute. Autopsies were performed with written informed consent from the patients or their relatives. The clinical diagnosis of AD was based on two major criteria: the Diagnostic and Statistical Manual of Mental Disorders: 4th Edition (DSM-IV) and the National Institute of Neurological and Communicational Disorders and Stroke-Alzheimer's Disease and Related Disorders Association (NINCDS-ADRDA). The neuropathological diagnosis of AD was made using Consortium to Establish a Registry for Alzheimer's Disease criteria (average age at death, 79.2 ± 4.4 years). Control brains were obtained from age-matched individuals with no history of neurological or psychiatric illness (average age at death, 80.4 ± 4.2 years). Subjects, age, gender, postmortem time, Braak stage, seizure history, and relative protein/tubulin ratios are indicated.

On the other hand, the present study showed that HCN1 physically associated with APP through the extracellular domain of APP. Therefore, HCN1-mediated regulation of Aβ generation may depend on a molecular linkage between HCN1 and APP and not simply on alterations in neuronal excitability. However, the molecular mechanism by which HCN1 potentially links epileptic seizures to Aβ generation in AD remains to be elucidated.

Our results suggest that ablation of X11/X11L induces aberrant HCN1 distribution and function along with epilepsy. Although the molecular mechanism by which X11s regulates HCN channel activity also remains unclear, X11s are known to modulate intracellular trafficking of membrane proteins. For example, X11s interact with certain proteins implicated in traffic and transport, such as Arfs, Rab6, and KIF17 [29,44,45]. Furthermore, X11s bind to vesicular cargo proteins, such as APP and alcadein [16,46,47] and regulate the intracellular distribution of APP [21,30]. We hypothesize that X11 and X11L similarly influence the trafficking and/or intracellular localization of HCN1. We further hypothesize that the mislocalization of HCN1 observed in X11^{-/-}/X11L^{-/-} mice (Additional file 1: Figure S4) may cause aberrant excitatory neuronal activities, resulting in epileptic seizures.

In conclusion, this study indicates that HCN1 may play an important role in the regulation of neuronal

activity, along with Aβ generation in the hippocampal formation. However, we cannot rule out the possibility that additional ion channels (e.g., M-channels, Kir-channels, and sodium leak channels) also participate in the regulation of APP metabolism. Taken together, the current observations may provide new insights into the mechanisms underlying the linkage between epileptic seizures and Aβ generation in AD.

Methods

Animals and human non-AD and AD brain samples

All animal studies were conducted in compliance with the guidelines of the Animal Studies Committees of Hokkaido University (Sapporo, Japan), Shiga University (Shiga, Japan), and the National Institute of Biomedical Innovation (Osaka, Japan). Mice were maintained under a 12-h light/12-h dark cycle (lights on, 7:00 A.M.–7:00 P.M.), and provided with food and water *ad libitum*. $X11^{-/-}/X11L^{+/+}$, $X11^{+/+}/X11L^{-/-}$, and $X11^{-/-}/X11L^{-/-}$ mice have already been described [20,21]. $HCN^{-/-}$ mice (stock number 005034) were purchased from The Jackson Laboratory (Bar Harbor, Maine). Male mice were used for all experiments.

Brain samples containing the superior temporal gyrus of cynomolgus monkeys (*Macaca fascicularis*) were obtained from Shiga University of Medical Science and the National Institute of Biomedical Innovation. The monkeys were housed in individual cages prior to the experiment and were maintained according to institutional guidelines for experimental animal welfare. Human brain samples containing the superior temporal gyrus (Broadmann area 22) were obtained from the Brain Bank for Aging Research, the Tokyo Metropolitan Institute of Gerontology (Itabashi, Tokyo, Japan). Human temporal cortical specimens for the quantification of proteins were obtained from brains that were removed, processed, and stored at –80°C within 16 h postmortem at the Brain Bank at Tokyo Metropolitan Institute of Gerontology. (Patients were placed in a cold (4°C) room within 2 h of death.) For all brains registered at the bank, written informed consent for their use for medical research was obtained from the patient prior to death or from the patient's family. Brain specimens were collected from Broadmann area 22 (superior temporal gyrus) for 12 AD patients (79.2±4.4 years of age) and 13 control patients (80.4±4.2 years of age) [48]. Detailed descriptions of all subjects, including the relative protein/tubulin ratio for each individual, are shown in Table 1.

Antibodies

Polyclonal rabbit anti-HCN1 antibody [25] and polyclonal rabbit anti-X11 UT153 antibody [21] have already been described. Monoclonal mouse anti-tubulin DM1A antibody and polyclonal rabbit anti-c-Fos, rabbit anti-Egr-1, and goat anti-HCN1 antibodies (sc-19706) were purchased from Santa Cruz Biotechnology (Santa Cruz, CA, USA). Characterization and demonstration of the antigen-specificity of the goat anti-HCN1 antibody (sc-19706) is shown in Additional file 1: Figure S7. Monoclonal mouse anti-X11L/mint2 and anti-PSD95 antibodies were purchased from BD Transduction Laboratories (Lexington, KY, USA). Anti-actin antibody and the anti-HCN1 antibody, AB5884, were purchased from Millipore (Billerica, MA, USA). Anti-FLAG M2 and polyclonal rabbit anti-APP cytoplasmic domain (N-terminus) antibodies were purchased from Sigma-Aldrich (St. Louis, MO, USA), and the anti-human APP extracellular domain antibody (LN27) was purchased from Zymed (San Francisco, CA, USA). Anti-FLAG M2 affinity gel and FLAG peptide were purchased from Sigma-Aldrich.

Plasmid construction

Human APP695 (hAPP695) and FLAG-APP695 cDNA were inserted into the pcDNA3 plasmid at the HindIII/XbaI restriction sites to produce pcDNA3-hAPP695 and pcDNA3-FLAG-hAPP695 [46]. The cDNA constructs pcDNA3-hAPP$_{Acyt}$ (in which amino acids 652–695 of hAPP695 are deleted) and pcDNA3.1-C99-FLAG (in which the signal sequence of hAPP is inserted into the 5' region of C99) were generated by PCR using pcDNA3-hAPP695 as the template. The generated fragments were ligated into pcDNA3-hAPP695 and pcDNA3.1-FLAG at the BamHI/XbaI restriction site and the HindIII/XbaI restriction site, respectively. The pCI-*murine* HCN1 vector was a kind gift from Dr. Takahiro M. Ishii [49].

Immunohistochemistry

Murine brain tissue sections were prepared and incubated with primary antibodies as described [21]. The sections were further incubated with goat anti-rabbit IgG antibodies conjugated to biotin (Vector Laboratories, Burlingame, CA, USA), followed by the ABC complex. Peroxidase activity was revealed using diaminobenzidine as the chromogen. Alternatively, sections were incubated with donkey anti-mouse IgG coupled with Alexa Fluor 488, donkey anti-rabbit IgG coupled with Cy3, or donkey anti-goat IgG coupled with Alexa Fluor 633 in phosphate buffered saline (PBS) containing 3% bovine serum albumin (BSA) for 2 h at room temperature. Sections were mounted onto slides with Shandon Immu-Mount (Thermo, Pittsburgh, PA, USA) and viewed under a BZ-9000 microscope (Keyence, Woodcliff Lake, NJ, USA).

Immunoblotting and co-immunoprecipitation analysis

The cortices of wild type, $X11^{-/-}/X11L^{+/+}$, $X11^{+/+}/X11L^{-/-}$, $X11^{-/-}/X11L^{-/-}$, $HCN1^{+/-}$, and $HCN1^{-/-}$ mice, and cynomolgus monkey brains (superior temporal gyrus) and human post-mortem brains (superior temporal gyrus) were homogenized in eight volumes of radioimmune

precipitation assay buffer containing 0.5% (w/v) sodium dodecyl sulfate (SDS) and a protease inhibitor mixture (5 µg/ml chymostatin, 5 µg/ml leupeptin, and 5 µg/ml pepstatin). The homogenates were lysed by sonication on ice and centrifuged at 20,000 × g for 10 min at 4°C. The resulting supernatants were used for immunoblot analysis. Proteins (10 µg per lysate) were separated via SDS (w/v) polyacrylamide gel electrophoresis (SDS-PAGE) on 7.5% (w/v) polyacrylamide gels.

The cortex (from one mouse) and EC-rich region (from five mice) from wild type and gene-null mice were homogenized in eight volumes of HBS-T lysis buffer (10 mM HEPES [pH 7.6] containing 150 mM NaCl, 5 mM EDTA, 0.5% [v/v] Triton X-100, 5 µg/ml chymostatin, 5 µg/ml leupeptin, and 5 µg/ml pepstatin A). Homogenates were then centrifuged at 20,000 × g for 10 min at 4°C. N2a cells (~1 × 10^6) were transiently transfected with 0.8 µg pcDNA3-FLAG-hAPP695, pcDNA3-hAPP695, pcDNA3-hAPP$_{Acyt}$, or pcDNA3.1-C99-FLAG and 0.4 µg of pCI-*murine* HCN1 using Lipofectamine 2000 (Invitrogen) and cultured for 24 h in medium (DMEM) containing 10% (v/v) fetal bovine serum (FBS). Cells were harvested, lysed in lysis buffer (PBS containing 1.0% [v/v] Triton X-100, 5 µg/ml chymostatin, 5 µg/ml leupeptin, and 5 µg/ml pepstatin A), and centrifuged for 5 min at 4°C. The resulting supernatants were incubated with anti-FLAG M2, anti-hAPP extracellular domain (LN27), anti-HCN1, anti-X11, or anti-X11L/Mint2 antibody at 4°C for 2 h. Each immunocomplex was recovered with Dynabeads® Protein G (Invitrogen) and washed three times with lysis buffer. The proteins were separated on 7.5% (w/v) polyacrylamide gels, transferred onto nitrocellulose membranes, and analyzed by immunoblotting with the indicated antibodies. The immunoreactants were detected using the ECL plus™ detection system (GE Healthcare, Houston, TX, USA) and quantified using a Versa Doc model 3000 (Bio-Rad, Hercules, CA, USA).

Affinity purification of FLAG-sAPP from N2a conditioned medium and immunoprecipitation of APP-HCN1 complex

N2a cells (~8.8 × 10^6) were transiently transfected with 5 µg pcDNA3-FLAG-hAPP695 using Lipofectamine 2000 (Invitrogen) and cultured for 24 h in 8 mL of medium (DMEM) containing 10% (v/v) FBS. FLAG-sAPP was collected from the conditioned culture medium by using 50 µL of anti-FLAG M2 affinity gel. The collected FLAG-sAPP that was bound to the gel was washed twice with wash buffer I (20 mM Tris–HCl [pH 8.0], 1 M NaCl, and 0.1% Triton X-100) and twice with wash buffer II (50 mM Tris–HCl [pH8.0], 150 mM NaCl, 1% Triton X-100, 0.05% SDS, and 5 mM EDTA). Collected FLAG-sAPP was then eluted from the affinity gel with 20 µg FLAG-peptide and subjected to immunoblotting and Coomassie brilliant blue (CBB) staining to ascertain the degree of purification.

FLAG-sAPP or FLAG-peptide coupled to anti-FLAG M2 affinity beads were then incubated for 2 h at 4°C with HBS-T-soluble lysates derived from wild type N2a cells or N2a cells transiently overexpressing HCN1. The beads were washed three times with HBS-T lysis buffer. The proteins bound to the beads were separated on 7.5% (w/v) polyacrylamide gels, transferred onto membranes, and analyzed by immunoblotting with the indicated antibodies. The immunoreactants were detected using the ECL plus™ detection system (GE Healthcare) and quantified using a Versa Doc model 3000 (Bio-Rad).

Quantification of Aβ40 and Aβ42

Endogenous murine Aβ was measured as described previously [21] using cortices dissected from 4-month-old mice. Murine Aβ40 and Aβ42 were measured using a sandwich ELISA (sELISA) system (mouse/rat Aβ40 and Aβ42 assay kit, Immuno-Biological Laboratories (IBL), Fujioka, Japan). N2a cells (~2 × 10^5) were transiently transfected with 0.2 µg pcDNA3-FLAG-hAPP695 and 0.1 µg pCI-*murine* HCN1 using Lipofectamine 2000 (Invitrogen) and cultured in medium (DMEM) containing 10% (v/v) FBS. After 24 h, cells were incubated in fresh medium for an additional 4 h with or without 10 µM ZD7288 (Tocris Bioscience, Bristol, UK). Human Aβ40 (hAβ40) and hAβ42 secreted into the culture medium during the 4-h incubation were quantified using the sELISA system.

Electroencephalogram recording

To obtain free-moving cortical electrocorticogram recordings, recording and reference electrodes were screwed onto the skull over the temporal (anterior = −3.1 mm, lateral = 2.5 mm, relative to bregma) and occipital regions of the murine brain. Recordings were continuously made using a cortical electroencephalogram linked to a telemetry system (Unimec, Usmate Velate, Italy) throughout the experiment [50].

Ih current recording

All experiments were performed in a blinded manner. Mice (12–14 weeks old) were anesthetized with halothane (Takeda Chemical Industries) and then sacrificed by decapitation. The brain was rapidly removed and immediately placed in a cold (4°C) cutting solution, which contained 234 mM sucrose, 2.5 mM KCl, 1.1 mM NaH$_2$PO$_4$, 10 mM MgSO$_4$, 26 mM NaHCO$_3$, 12 mM glucose, and 0.5 mM CaCl$_2$. Horizontal slices (300 µm thick), which included the EC and the hippocampus, were prepared using a vibratome (VT1000S, Leica, Nussloch, Germany). During recording, individual slices were transferred to a submerged recording chamber and continuously perfused with artificial cerebrospinal fluid (ACSF) maintained at 30–32°C. The ACSF contained 125 mM

NaCl, 2.5 mM KCl, 1.1 mM NaH_2PO_4, 1.0 mM $MgSO_4$, 26 mM $NaHCO_3$, 12 mM glucose, and 2.0 mM $CaCl_2$ and was saturated with 95% O_2 and 5% CO_2. Whole-cell patch-clamp recordings were obtained from principal excitatory cells in layer II of the EC. The patch pipettes were filled with an intracellular solution containing 30 mM K-methanesulfonate, 6 mM NaCl, 0.2 mM EGTA, 10 mM HEPES, 4 mM Mg-ATP, 0.3 mM Na_3-GTP, and 10 mM phosphocreatine-Tris (pH 7.3). In layer II cells of the EC, the hyperpolarization-induced and "slowly-activating" inward currents in the voltage-clamp mode mainly consisted of Ih currents [51]. When Ih currents were studied in the voltage-clamp mode, membrane potentials were first held at –65 mV, and then voltage steps with a duration of 7 s were applied from –55 mV to –125 mV (10 mV increments), after which the holding potentials were allowed to return to –65 mV to obtain the tail currents. The amplitudes of the tail currents at 50 ms after the end of the final voltage step were analyzed to obtain the Ih currents. In all electrophysiological analyses, pooled data were represented as the mean ± SEM.

Statistical analysis

Statistical analyses were performed using a two-tailed Mann–Whitney U-test, a one-way analysis of variance followed by Tukey's multiple comparison test, or the two-tailed Pearson's correlation coefficient. All analyses were conducted with GraphPad Prism 5 software.

Additional files

Additional file 1: Figure S1. Simultaneous recording of electrocorticogram in epilepsy model mice and corresponding movie. A representative electrocorticogram recorded during the interictal period in 13-week-old X11$^{-/-}$/ X11L$^{-/-}$ mice (n = 4) is shown. The underlined region indicates the time frame of the corresponding movie (Movie S3). **Figure S2.** Individual data of Ih currents density in entorhinal cortex layer II neurons of wild-type and X11s-null mice. (A) Indicidual data of Ih current density. Blue indicate the data of mouse #1 and red indicate mouse #2. (B) Mean, SD, SEM, and count number of A. P Value of Student's t-test (#1 vs #2) shown in bottom line. (C) Distribution and average of current density of A. Closed symbols indicate the data of mouse #1 and opened symbols indicate mouse #2 (mean ± SEM). **Figure S3.** HCN1 levels in the EC-rich region of the brains of X11$^{+/+}$/X11L $^{+/+}$ and X11s mutant mice. (A) Isolation of the EC-rich region from a horizontal slice (300 μm thick) of murine brain. Brain slices from 13-week-old X11$^{+/+}$/X11L$^{+/+}$, X11$^{+/+}$/X11L$^{-/-}$, X11$^{-/-}$/X11L$^{+/+}$, and X11$^{-/-}$/X11L$^{-/-}$ mice were prepared in ice-cold PBS using a vibratome (VT1200S; Leica) (left panel). The EC-rich region (EC) was separated from each slice as indicated (right panel). (B, C) Quantification of HCN1 in the EC-rich region. Horizontal slices were homogenized in eight volumes of radioimmune precipitation assay buffer containing 0.5% (w/v) SDS and a protease inhibitor mixture (5 μg/ml chymostatin, 5 μg/ml leupeptin, and 5 μg/ml pepstatin), subjected to sonication on ice, and centrifuged at 20,000 × g for 10 min at 4°C. (B) The resulting supernatants (each containing 10 μg protein) were analyzed by SDS-PAGE on 7.5% (w/v) polyacrylamide gels, followed by immunoblotting with anti-HCN1, anti-X11, anti-X11L, and anti-tubulin antibodies (n = 4). (C) The HCN1 level was normalized to the tubulin level to give the relative HCN1/tubulin ratio for each genotype (mean ± SEM, n = 4). **Figure S4.** Altered

distribution of the HCN channel in X11$^{-/-}$/X11L$^{-/-}$ mice. (A) Low-power images of horizontal brain sections from 13-week-old wild type (X11$^{+/+}$/X11L$^{+/+}$: upper panels) and X11$^{-/-}$/X11L$^{-/-}$ (Lower panels) mutant mice were immunostained with an anti-HCN1 antibody (n=3). Scale bar, 300 μm. (B) Representative high-resolution images of horizontal brain sections from 13-week-old X11$^{+/+}$/X11L$^{+/+}$ (a, c) and X11$^{-/-}$/X11L$^{-/-}$ (b, d) mice were subjected to immunostaining with an anti-HCN1 antibody (a, b) and Nissl stain (c, d). (C) Quantitative analysis of HCN1 immunoreactivity in the EC of 13-week-old wild type (X11$^{+/+}$/X11L$^{+/+}$) and X11$^{-/-}$/X11L$^{-/-}$ mutant mice. The intensity of the HCN1 immunoreactivity in the areas enclosed by the open boxes in A was measured using NIH Image J software. Scale bar, 50 μm. **Figure S5.** Complex formation of HCN1 with APP in N2a cells treated with ZD7288. FLAG-APP and HCN1 were transiently overexpressed in N2a cells ($\sim$1 × 10^6) with (+) or without (–) 10 μM ZD7288. To standardize the amount of plasmid transfected into the cells, an empty vector (–) was added to yield 1.2 μg of plasmid in total. The cell lysates were subjected to immunoprecipitation with anti-FLAG M2 antibody. Immunocomplexes were detected by immunoblotting with anti-HCN1 and anti-FLAG antibodies. **Figure S6.** Covariance analysis of various protein levels in the brain of cynomolgus monkeys. (A–H) Levels of HCN1, APP, Aβ40, and Aβ42 in the brain (superior temporal gyrus) of 4–37-year-old cynomolgus monkeys were quantified by immunoblotting and sELISA assay. Protein levels were normalized to tubulin levels or to tissue weight to give the relative protein/tubulin ratio for immunoblotting and the relative protein/tissue weight ratio for sELISA. (A) Correlation between age and APP level (n = 39, r = 0.8156, ****p < 0.0001). (B) Correlation between HCN1 and APP levels (n = 39, r = –0.3796, **p = 0.0086). (C, D) Correlation between HCN1 and Aβ40 levels (n = 39, r = –0.2878, *p = 0.0421). An enlarged view of (C) in the 0 to 1,000 f mol/mg tissue range is shown in (D) (E, F) Correlation between HCN1 and Aβ42 levels (n = 39, r = –0.2913, *p = 0.0401). An enlarged view of (E) in the 0 to 400 f mol/mg tissue range is shown in (F). (G) Correlation between APP and Aβ40 (n = 39, r = 0.2993, p = 0.072). (H) Correlation between APP and Aβ42 levels (n = 39, r = 0.3714, *p = 0.0236). Statistical analysis was performed using the two-tailed Pearson's correlation coefficient. **Figure S7.** Specificity of the polyclonal goat anti-HCN1 antibody. (A) Competition analysis using glutathione-S-transferase (GST) fused to the 60-amino acid carboxyl terminal region of murine HCN1 (mHCN1 C60). This region of the protein contains the epitope for the goat anti-HCN1 antibody used in this study (sc-19706; Santa Cruz Biotechnology). Brain lysates (10 μg protein) derived from HCN1$^{+/+}$ and HCN1$^{-/-}$ mice and cynomolgus monkeys were subjected to immunoblot analysis. The anti-HCN1 antibody was pre-incubated with 20 μg GST alone or GST-mHCN1 C60 recombinant protein at 4°C for 2 h. The pre-incubated antibody was then reacted with the immunoblots. HCN1 was detected in HCN1$^{+/+}$ mouse and monkey brains when the antibody was pre-incubated with GST alone, but not when the antibody was pre-incubated with GST-mHCN1 C60. (B) Titer comparison between anti-HCN1 antibodies. Brain lysates (10 μg protein) were subjected to immunoblot analysis with two commercial anti-HCN1 antibodies (sc-19706, Santa Cruz Biotechnology; and AB5884, Millipore). (C) Specificity of goat anti-HCN1 antibody (sc-19706) for immunohistochemical analysis. (a, b) Representative images of horizontal brain sections showing the hippocampal formation in 13-week-old HCN1$^{+/+}$ (a) and HCN1$^{-/-}$ (b) mice stained with goat anti-HCN1 antibody, followed by donkey anti-goat IgG coupled with FITC. (c, d) Magnified view of the squares in (a) and (b). HCN1 signals (green) observed in HCN1$^{+/+}$ mice were absent in HCN1$^{-/-}$ mice. Nuclei counter-stained with DAPI are shown in blue. Scale bars, 300 μm (a, b), 50 μm (c, d).

Additional file 2: Movie S1. Spontaneous epileptic seizures in X11$^{-/-}$/X11L$^{-/-}$ mice. The electrocorticogram of Supplementary Figure S1 and Movie S3 were simultaneously recorded.

Additional file 3: Movie S2. Spontaneous epileptic seizures in X11$^{-/-}$/X11L$^{-/-}$ mice. The electrocorticogram of Supplementary Figure S1 and Movie S3 were simultaneously recorded.

Additional file 4: Movie S3. Spontaneous epileptic seizures in X11$^{-/-}$/X11L$^{-/-}$ mice. The electrocorticogram of Supplementary Figure S1 and Movie S3 were simultaneously recorded.

Abbreviations

ACSF: Artificial cerebrospinal fluid; AD: Alzheimer's disease; APP: Amyloid precursor protein; Aβ: Amyloid β peptide; DG: Dentate gyrus; EC: Entorhinal cortex; FBS: Fetal bovine serum; HCN channel: Hyperpolarization-activated cyclic nucleotide gated channel; Ih current: Hyperpolarization-activated current; PBS: Phosphate buffered saline; sAPP: Soluble APP; SDS: Sodium dodecyl sulfate; sELISA: Sandwich ELISA; SDS-PAGE: SDS polyacrylamide gel electrophoresis; TBS: Tris buffere saline; X11L: X11-like; X11L2: X11-like2; X11s: X11 proteins.

Competing interests

The authors declare no competing interests.

Authors' contributions

YS, TI, GZ, MO, KI, SK and TS generated the hypotheses for the mouse, monkey and human projects. YS and TS drafted the manuscript. YS, TI, GZ, MO, MN, SK, RS, KI, and TS edited the manuscript and contributed to discussion. YS and NK performed the biochemical and histochemical analyses for the mouse and monkey studies. YS, MN and SM performed biochemical analyses for the human study. TI and KI conducted electrophysiological analyses for the mouse study. YS, GZ, MO and SK performed electroencephalogram recordings. MN and NK provided monkey tissues, and SM provided human tissues. All authors read and approved the final manuscript.

Author details

[1]Laboratory of Neuroscience, Graduate School of Pharmaceutical Sciences, Hokkaido University, Kita12-Nishi6, Kita-ku, Sapporo 060-0812, Japan. [2]Laboratory of Neurobiophysics, Graduate School of Medicine, Dentistry and Pharmaceutical Sciences, Okayama University, Okayama 700-8530, Japan. [3]Department of Psychiatry, The First Affiliated Hospital of China Medical University, Shenyang 110001, China. [4]Division of Neuroscience, Graduate School of Medicine, Mie University, Tsu 514-8507, Japan. [5]Molecular Neuroscience Research Center, Shiga University of Medical Science, Otsu 520-2192, Japan. [6]Laboratory of Disease Control, Tsukuba Primate Research Center, National Institute of Biomedical Innovation, Tsukuba 305-0843, Japan. [7]Department of Neuropathology, Tokyo Metropolitan Institute of Gerontology, Itabashi-ku, Tokyo 173-0015, Japan. [8]Brain Bank for Aging Research, Tokyo Metropolitan Institute of Gerontology, Itabashi-ku, Tokyo 173-0015, Japan. [9]Departments of Neuropsychiatry, Graduate School of Medicine, Hirosaki University, Hirosaki 036-8562, Japan. [10]Division of Cerebral Structure, National Institute for Physiological Sciences, Okazaki 444-8585, Japan. [11]Department of Information Physiology, National Institute for Physiological Sciences, Okazaki 444-8787, Japan.

References

1. Selkoe DJ: Alzheimer's disease is a synaptic failure. *Science* 2002, 298:789–791.
2. Hauser WA, Morris ML, Heston LL, Anderson VE: Seizures and myoclonus in patients with Alzheimer's disease. *Neurology* 1986, 36:1226–1230.
3. Hesdorffer DC, Hauser WA, Annegers JF, Kokmen E, Rocca WA: Dementia and adult-onset unprovoked seizures. *Neurology* 1996, 46:727–730.
4. Mendez M, Lim G: Seizures in elderly patients with dementia: epidemiology and management. *Drugs Aging* 2003, 20:791–803.
5. Amatniek JC, Hauser WA, DelCastillo Castaneda C, Jacobs DM, *et al*: Incidence and predictors of seizures in patients with Alzheimer's disease. *Epilepsia* 2006, 47:867–872.
6. Lozsadi DA, Larner AJ: Prevalence and causes of seizures at the time of diagnosis of probable Alzheimer's disease. *Dement Geriatr Cogn Disord* 2006, 22:121–124.
7. Marcon G, Giaccone G, Cupidi C, Balestrieri M, Beltrami CA, *et al*: Neuropathological and clinical phenotype of an Italian Alzheimer family with M239V mutation of presenilin 2 gene. *J Neuropathol Exp Neurol* 2004, 63:199–209.
8. Kamenetz F, Tomita T, Hsieh H, Seabrook G, Borchelt D, *et al*: APP processing and synaptic function. *Neuron* 2003, 37:925–937.
9. Cirrito JR, Yamada KA, Finn MB, Sloviter RS, Bales KR, *et al*: Synaptic activity regulates interstitial fluid amyloid-beta levels in vivo. *Neuron* 2005, 48:913–922.
10. Cirrito JR, Kang JE, Lee J, Stewart FR, Verges DK, *et al*: Endocytosis is required for synaptic activity-dependent release of amyloid-beta in vivo. *Neuron* 2008, 58:42–51.
11. Postea O, Biel M: Exploring HCN channels as novel drug targets. *Nat Rev Drug Discov* 2011, 10:903–914.
12. Noam Y, Bernald C, Baram TZ: Towards an integrated view of HCN channel role in epilepsy. *Curr Opin Neurobiol* 2011, 21:873–879.
13. Kimura K, Kitano J, Nakajima Y, Nakanishi S: Hyperpolarization-activated cyclic nucleotide-gated HCN2 cation channel forms a protein assembly with multiple neuronal scaffold proteins in distinct modes of protein-protein interaction. *Genes Cells* 2004, 9:631–640.
14. Suzuki T, Nakaya T: Regulation of amyloid β-protein precursor by phosphorylation and protein interaction. *J Biol Chem* 2008, 283:29633–29637.
15. Borg JP, Yang Y, De Taddeo Borg M, Margolis B, Turner RS: The X11alpha protein slows cellular amyloid precursor protein processing and reduces Abeta40 and Abeta42 secretion. *J Biol Chem* 1998, 273:14761–14766.
16. Tomita S, Ozaki T, Taru H, Oguchi S, Takeda S, *et al*: Interaction of a neuron-specific protein containing PDZ domains with Alzheimer's amyloid precursor protein. *J Biol Chem* 1999, 274:2243–2254.
17. Lee JH, Lau KF, Perkinton MS, Standen CL, Shemilt SJ, *et al*: The Neuronal Adaptor Protein X11α Reduces Aβ Levels in the Brains of Alzheimer's APPswe Tg2576 Transgenic Mice. *J Biol Chem* 2003, 278:47025–47029.
18. Lee JH, Lau KF, Perkinton MS, Standen CL, Rogelj B, *et al*: The neuronal adaptor protein X11beta reduces amyloid beta-protein levels and amyloid plaque formation in the brains of transgenic mice. *J Biol Chem* 2004, 279:49099–49104.
19. Mitchell JC, Ariff BB, Yates DM, Lau KF, Perkinton MS, *et al*: X11beta rescues memory and long-term potentiation deficits in Alzheimer's disease APPswe Tg2576 mice. *Hum Mol Genet* 2009, 18:4492–4500.
20. Sano Y, Syuzo-Takabatake A, Nakaya T, Saito Y, Tomita S, *et al*: Enhanced amyloidogenic metabolism of the amyloid beta-protein precursor in the X11L-deficient mouse brain. *J Biol Chem* 2006, 281:37853–37860.
21. Saito Y, Sano Y, Vassar R, Gandy S, Nakaya T, *et al*: X11 proteins regulate the translocation of amyloid beta-protein precursor (APP) into detergent-resistant membrane and suppress the amyloidogenic cleavage of APP by beta-site-cleaving enzyme in brain. *J Biol Chem* 2008, 283:35763–35771.
22. Kondo M, Shiono M, Itoh G, Takei N, Matsushima T, *et al*: Increased amyloidogenic processing of transgenic human APP in X11-like deficient mouse brain. *Mol Neurodegener* 2010, 5:35.
23. Morimoto K, Fahnestock M, Racine RJ: Kindling and status epilepticus models of epilepsy: rewiring the brain. *Prog Neurobiol* 2004, 73:1–60.
24. van Strien NM, Cappaert NL, Witter MP: The anatomy of memory: an interactive overview of the parahippocampal-hippocampal network. *Nat Rev Neurosci* 2009, 10:272–282.
25. Notomi T, Shigemoto R: Immunohistochemical localization of Ih channel subunits, HCN1-4, in the rat brain. *J Comp Neurol* 2004, 471:241–276.
26. Ludwig A, Budde T, Stieber J, Moosmang S, Wahl C, *et al*: Absence epilepsy and sinus dysrhythmia in mice lacking the pacemaker channel HCN2. *EMBO J* 2003, 22:216–224.
27. Huang Z, Walker MC, Shah MM: Loss of dendritic HCN1 subunits enhances cortical excitability and epileptogenesis. *J Neurosci* 2009, 29:10979–10988.

28. Nolan MF, Dudman JT, Dodson PD, Santoro B: HCN1 channels control resting and active integrative properties of stellate cells from layer II of the entorhinal cortex. *J Neurosci* 2007, 27:12440–12451.
29. Setou M, Nakagawa T, Seog DH, Hirokawa N: Kinesin superfamily motor protein KIF17 and mLin-10 in NMDA receptor-containing vesicle transport. *Science* 2000, 288:1796–1802.
30. Saito Y, Akiyama M, Araki Y, Sumioka A, Shiono M, *et al*: Intracellular Trafficking of the Amyloid β-Protein Precursor (APP) Regulated by Novel Function of X11-Like. *PLoS One* 2011, 6:e22108.
31. Braak H, Braak E: Neuropathological stageing of Alzheimer-related changes. *Acta Neuropathol* 1991, 82:239–259.
32. Nakamura S, Nakayama H, Goto N, Ono F, Sakakibara I, Yoshikawa Y: Histopathological studies of senile plaques and cerebral amyloidosis in cynomolgus monkeys. *J Med Primatol* 1998, 27:244–252.
33. Oikawa N, Kimura N, Yanagisawa K: Alzheimer-type tau pathology in advanced aged nonhuman primate brains harboring substantial amyloid deposition. *Brain Res* 2010, 1315:137–149.
34. Podlisny MB, Tolan DR, Selkoe DJ: Homology of the amyloid β protein precursor in monkey and human supports a primate model for β amyloidosis in Alzheimer's disease. *Am J Pathol* 1991, 138:1423–1435.
35. Rogelj B, Mitchell JC, Miller CCJ, McLoughlin DM: The X11/Mint family of adaptor proteins. *Brain Res Rev* 2006, 52:305–315.
36. Shah MM, Anderson AE, Leung V, Lin X, Johnston D: Seizure-induced plasticity of h channels in entorhinal cortical layer III pyramidal neurons. *Neuron* 2004, 44:495–508.
37. Powell KL, Ng C, O'Brien TJ, Xu SH, Williams DA, *et al*: Decreases in HCN mRNA expression in the hippocampus after kindling and status epilepticus in adult rats. *Epilepsia* 2008, 49:1686–1695.
38. Bender RA, Soleymani SV, Brewster AL, Nguyen ST, Beck H, *et al*: Enhanced expression of a specific hyperpolarization-activated cyclic nucleotide-gated cation channel (HCN) in surviving dentate gyrus granule cells of human and experimental epileptic hippocampus. *J Neurosci* 2003, 23:6826–6836.
39. Brewster A, Bender RA, Chen Y, Dube C, Eghbal Ahmadi M, Baram TZ: Developmental febrile seizures modulate hippocampal gene expression of hyperpolarization-activated channels in an isoform- and cell-specific manner. *J Neurosci* 2002, 22:4591–4599.
40. Dugladze T, Vida I, Tort AB, Gross A, Otahal J, *et al*: Impaired hippocampal rhythmogenesis in a mouse model of mesial temporal lobe epilepsy. *Proc Natl Acad Sci USA* 2007, 104:17530–17535.
41. Jung S, Jones TD, Lugo JN Jr, Sheerin AH, Miller JW, *et al*: Progressive dendritic HCN channelopathy during epileptogenesis in the rat pilocarpine model of epilepsy. *J Neurosci* 2007, 27:13012–13021.
42. Shin M, Brager D, Jaramillo TC, Johnston D, Chetkovich DM: Mislocalization of h channel subunits underlies h channelopathy in temporal lobe epilepsy. *Neurobiol Dis* 2008, 32:26–36.
43. Marcelin B, Chauviere L, Becker A, Migliore M, Esclapez M, Bernard C: h channel-dependent deficit of theta oscillation resonance and phase shift in temporal lobe epilepsy. *Neurobiol Dis* 2009, 33:436–447.
44. Nie Z, Hirsch DS, Randazzo PA: Arf and its many interactors. *Curr Opin Cell Biol* 2003, 15:396–404.
45. Teber I, Nagano F, Kremerskothen J, Bilbilis K, Goud B, Barnekow A: Rab6 interacts with the mint3 adaptor protein. *Biol Chem* 2005, 386:671–677.
46. Araki Y, Tomita S, Yamaguchi H, Miyagi N, Sumioka A, *et al*: Novel cadherin-related membrane proteins, Alcadeins, enhance the X11-like protein-mediated stabilization of amyloid beta-protein precursor metabolism. *J Biol Chem* 2003, 278:49448–49458.
47. Araki Y, Kawano T, Taru H, Saito Y, Wada S, *et al*: The novel cargo Alcadein induces vesicle association of kinesin-1 motor components and activates axonal transport. *EMBO J* 2007, 26:1475–1486.
48. Kakuda N, Shoji M, Arai H, Furukawa K, Ikeuchi T, *et al*: Altered γ-secretase activity in mild cognitive impairment and Alzheimer's disease. *EMBO Mol Med* 2012, 4:344–352.
49. Ishii TM, Takano M, Ohmori H: Determinants of activation kinetics in mammalian hyperpolarization-activated cation channels. *J Physiol* 2001, 537:99–100.
50. Zhu G, Okada M, Yoshida S, Ueno S, Mori F, *et al*: Rats harboring S284L Chrna4 mutation show attenuation of synaptic and extrasynaptic GABAergic transmission and exhibit the nocturnal frontal lobe epilepsy phenotype. *J Neurosci* 2008, 28:12465–12376.
51. Dickson CT, Magistretti J, Shalinsky MH, Fransen E, Hasselmo ME, Alonso A: Properties and role of I(h) in the pacing of subthreshold oscillations in entorhinal cortex layer II neurons. *J Neurophysiol* 2000, 83:2562–2579.

ORIGINAL ARTICLE

Mutational analysis of familial and sporadic amyotrophic lateral sclerosis with *OPTN* mutations in Japanese population

HIROYA NARUSE[1], YUJI TAKAHASHI[1], TAMEKO KIHIRA[2], SOHEI YOSHIDA[2], YASUMASA KOKUBO[3], SHIGEKI KUZUHARA[4], HIROYUKI ISHIURA[1], MASAHARU AMAGASA[5], SHIGEO MURAYAMA[6], SHOJI TSUJI[1] & JUN GOTO[1]

[1]*Department of Neurology, Graduate School of Medicine, The University of Tokyo, Tokyo,* [2]*Kansai University of Health Sciences, Kumatori, Osaka,* [3]*Department of Neurology, Mie University School of Medicine, Tsu, Mie,* [4]*Department of Medical Welfare, Suzuka University of Medical Science, Suzuka, Mie,* [5]*Department of Neurology and Neurosurgery, Yamagata Tokushukai Hospital, Yamagata, and* [6]*Geriatric Neuroscience (Neuropathology), Tokyo Metropolitan Institute of Gerontology, Tokyo, Japan*

Abstract

Our objective was to elucidate the genetic epidemiology of familial amyotrophic lateral sclerosis (FALS) and sporadic ALS (SALS) with *OPTN* mutations in the Japanese population. Mutational analysis of *OPTN* was conducted in 18 FALS pedigrees in whom mutations in other causative genes have been excluded and in 218 SALS patients by direct nucleotide sequence analysis. Novel non-synonymous variants identified in ALS patients were further screened in 271 controls. Results showed that although no mutations were identified in the FALS pedigrees, a novel heterozygous non-synonymous variant c.481G>A (p.V161M) was identified in one SALS patient, who originated from the southern-most part of the Kii Peninsula. The mutation was not present in 271 controls. As the clinical feature, the patient carrying V161M showed predominantly upper motor neuron signs with slow progression. This study suggests that mutations in *OPTN* are not the main cause of ALS in the Japanese population.

Key words: *Motor neuron disease, amyotrophic lateral sclerosis, OPTN mutation, genetic analysis, V161M*

Introduction

Molecular genetic research on amyotrophic lateral sclerosis (ALS) has revealed a number of causative genes for familial ALS (FALS), which include *SOD1* (1), *ALS2* (2,3), *DCTN1* (4), *VAPB* (5), *CHMP2B* (6), *ANG* (7), *TARDBP* (8), and *FUS* (9,10). These genes collectively account for approximately 30% of FALS pedigrees (11). Mutations in these genes have also been identified in some sporadic ALS (SALS) patients, suggesting mutations with reduced penetrance or *de novo* mutations (12,13). Recently, hexa-nucleotide repeat expansion within the *C9ORF72* gene has been reported to be associated with a large proportion of cases of ALS and frontotemporal dementia (FTD) with wider European ancestry (14–16). Mutations in *UBQLN2* were also identified to cause dominant X-linked juvenile and adult-onset ALS and ALS/dementia (17). *OPTN*, which was

previously identified as the causative gene for rare autosomal dominant familial primary open-angle glaucoma (POAG), has been reported as the causative gene for autosomal dominant and auto-somal recessive FALS (18). Subsequent genetic epidemiological studies on *OPTN* mutations in different cohorts have revealed that frequencies of mutations in patients with FALS and SALS vary among cohorts, from 0% to 4.35% (pedigree frequency) in those with FALS, and from 0% to 3.54% (case frequency) in those with SALS (18–23). Further analyses on larger cohorts of various ethnic backgrounds will be necessary to establish the genetic epidemiology and clinical characteristics of ALS and the genotype-phenotype correlations of ALS with *OPTN* mutations. We conducted further mutational analysis of *OPTN* in our cohorts to establish the molecular epidemiology of ALS in patients with mutations in *OPTN*.

Materials and methods

Thirty-five FALS pedigrees, 218 SALS patients, and 271 controls, all of whom were from the Japanese population, were enrolled in this study. Of the 35 FALS pedigrees, 17 harbored causative mutations in other causative genes for FALS with the autosomal dominant mode of inheritance. The remaining 18 pedigrees consisted of 13 with the autosomal dominant mode of inheritance, two pedigrees with affected sibs with consanguinity, and three pedigrees with affected sibs without consanguinity. The 218 SALS patients, most of whom visited the University of Tokyo Hospital, included 33 from Yamagata Prefecture, on the northern part of Honshu island, and 15 from the Kii Peninsula, on the southern part of Honshu island. The mean age at onset of the SALS cohort was 58.9 years, and the male: female ratio was 3: 2. All of the genomic DNA samples were obtained from the participants of this study with their written informed consent, and this research was approved by the Institutional Review Board of the University of Tokyo.

Mutational analysis

Mutations in causative genes for FALS were analyzed employing a DNA microarray-based resequencing system as described elsewhere (24) or a direct nucleotide sequencing method conducted using a BigDye Terminator ver. 3.1 cycle sequencing kit on a 3100 ABI Prism Genetic Analyzer (Applied Biosystems). All the coding exons of *OPTN* (exons 4–16) were amplified by genomic PCR using specific primers for each exon recently reported (18) and further subjected to direct nucleotide sequence analysis.

Mutations in other causative genes for FALS, including *SOD1*, *ALS2*, *DCTN1*, *VAPB*, *CHMP2B*, *ANG*, and *TARDBP*, were firstly excluded employing a DNA microarray-based resequencing system. Secondary, mutational analysis of *FUS* employing a direct nucleotide sequencing method was performed. The remaining samples were subjected to mutational analysis of *OPTN* by direct nucleotide sequence analysis.

The variants identified by the mutational analysis were evaluated using databases of dbSNP (http://www.ncbi.nlm.nih.gov/SNP/index.html), 1000 Genomes Project (http://www.1000genomes.org/), and Exome Sequencing Project (https://esp.gs.washington.edu/). When novel non-synonymous variants not registered in these databases were identified, they were further screened in 271 controls by direct nucleotide sequence analysis. The effect of amino acid changes caused by identified novel variants was predicted using the PolyPhen-2 website (http://genetics.bwh.harvard.edu/pph2/).

Results

Of the 35 FALS pedigrees enrolled in this study, 17 harbored causative mutations in other causative genes for FALS including 14 *SOD1*, two *FUS*, and one *TARDBP*. The remaining 18 pedigrees were subjected to mutational analysis of *OPTN*. Five variants including four known SNPs and a novel synonymous variant in exon 16 were identified (Table I). We did not observe any causative mutations in *OPTN* in the FALS pedigrees in our cohort.

In the 218 SALS patients, seven variants including four known SNPs, two novel synonymous variants in exons 4 and 7, and one novel non-synonymous variant in exon 6 not registered in dbSNPs, 1000 Genomes Project, or Exome Sequencing Project were identified (Table II). Known causative mutations for ALS were not identified in the SALS patients. The novel heterozygous non-synonymous variant of c.481G >A in exon 6 substituting methionine for valine at amino acid position 161 (p.V161M) was identified in a SALS patient (Figure 1A, B). This novel variant of V161M was not present in 271 controls (542 chromosomes). Although the amino acid valine at position 161 was not necessarily highly conserved among species (Figure 1C), the PolyPhen-2 prediction was possibly damaging with a score of 0.913.

Interestingly, the patient with V161M mutation originated from the southernmost part of the Kii Peninsula, where the prevalence of ALS is high and patients with the ALS-parkinsonism-dementia

Table I. Summary of *OPTN* variants identified in 18 FALS patients.

Exon	SNP ID*	Base changes	Annotation	Amino acid changes	Number of pedigrees (Allele frequency)		Allele frequency (1000 Genomes)**
4	rs2234968	c.102G>A	Synonymous		3 homozygotes, 1 heterozygote#	(0.389)	0.182
5	rs11258194	c.293T>A	Non-synonymous	p.Met98Lys	1 heterozygote	(0.028)	0.110
10	rs523747	c.964A>G	Non-synonymous	p.Lys322Glu	18 homozygotes	(1.000)	1.000
16	rs75654767	c.1634G>A	Non-synonymous	p.Arg545Gln	2 heterozygotes#	(0.056)	0.028
16	Novel	c.1713C>T	Synonymous		1 heterozygote	(0.028)	0.000

*SNP ID is the single-nucleotide polymorphism identification obtained from dbSNP database.
**The allele frequencies in East Asian populations were obtained from 1000 Genomes Project (http://www.1000genomes.org/).
#One patient carried both the heterozygous c.102G>A variant and the heterozygous c.1634G>A variant.

RIGHTS LINK

Table II. Summary of *OPTN* variants identified in 218 SALS patients.

Exon	SNP ID*	Base changes	Annotation	Amino acid changes	Number of cases (Allele frequency)		Allele frequency (1000 Genomes)**
4	rs2234968	c.102G>A	Synonymous		3 homozygotes, 59 heterozygotes	(0.149)	0.182
4	Novel	c.147C>T	Synonymous		1 homozygote	(0.004)	0.000
5	rs11258194	c.293T>A	Non-synonymous	p.Met98Lys	17 heterozygotes	(0.039)	0.110
6	Novel	c.481G>A	Non-synonymous	p.Val161Met	1 heterozygote	(0.002)	0.000
7	Novel	c.630A>T	Synonymous		1 heterozygote	(0.002)	0.000
10	rs523747	c.964A>G	Non-synonymous	p.Lys322Glu	218 homozygotes	(1.000)	1.000
16	rs75654767	c.1634G>A	Non-synonymous	p.Arg545Gln	13 heterozygotes	(0.030)	0.028

*SNP ID is the single-nucleotide polymorphism identification obtained from dbSNP database.
**The allele frequencies in East Asian populations were obtained from 1000 Genomes Project (http://www.1000genomes.org/).

complex are clustered. We further conducted the mutational analysis of *OPTN* recruiting four additional patients with SALS in the same district. These patients, however, harbored neither the V161M mutation nor any other mutations in *OPTN*.

The clinical features of the patient with the V161M mutation are briefly presented as follows. The patient was a 35-year-old male at the time of diagnosis of ALS, who developed upper extremity weakness for one year. Weakness and atrophy predominantly in upper extremities gradually worsened. Neurological examination at the age of 39 years revealed tongue atrophy and fasciculation, attenuated tendon reflexes and muscle wasting in the upper extremities, and enhanced tendon reflexes in the lower extremities with bilateral extensor plantar reflexes. He became mechanical-ventilator-dependent at the age of 50 years. There was no evidence of parkinsonism or cognitive impairment at the age of 50 years. His medical history included unexplained vision loss of his right eye in his childhood. His father, who also originated from the southernmost part of the Kii Peninsula, was alive and did not show any symptoms indicative of motor neuron disease when the index patient was 35 years old. His mother, who originated from southeastern part of the Kii Peninsula, died of liver cirrhosis, but her age at death was not indicated.

Discussion

In this study, we conducted a comprehensive mutational analysis of *OPTN* in a large cohort of Japanese FALS and SALS patients. Among our 35 FALS pedigrees, 17 families had mutations in other causative genes previously reported, as described in Results, and we did not find any causative mutations in *OPTN* in the remaining 18 pedigrees. On the other hand, among the 218 patients with SALS, we identified a patient carrying a novel non-synonymous mutation of *OPTN*.

Previous genetic studies on *OPTN* mutations in different cohorts have demonstrated that the frequencies of *OPTN* mutations are from 0% to 4.35% (pedigree frequency) in FALS (18–23) (Table IIIA). *OPTN* was initially identified as a causative gene for FALS in a consanguineous pedigree through homozygosity mapping followed by sequencing of candidate genes in the homozygous region. In our cohort, autosomal recessive inheritance was suggested in only five of the 35 FALS families, which may account for the fact that we did not identify any causative mutations in *OPTN* in the FALS families. Since the number of families enrolled in this study is limited, further extensive mutational analysis of larger cohorts of FALS will be necessary to establish the genetic epidemiology of FALS patients with *OPTN* mutations.

In our SALS cohort, a novel heterozygous non-synonymous variant, V161M, was identified in a patient. Previous genetic studies on *OPTN* mutations in different cohorts have shown a number of heterozygous missense mutations in SALS patients (20,21) and that the frequencies of *OPTN* mutations are from 0% to 3.54% (case frequency) in SALS (18–23) (Table IIIB). When we assess the implication of the
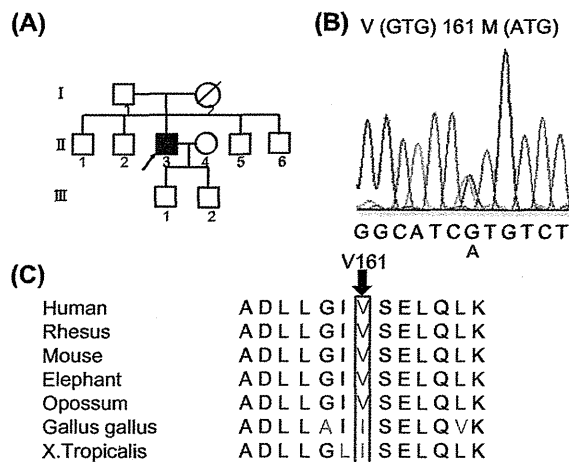

Figure 1. (A) Pedigree chart of patient with V161M variant in *OPTN*. Affected individuals are indicated by filled symbols. The proband is indicated by an arrow. Unaffected individuals are indicated by open symbols. Slashed symbols indicate deceased subjects. Ages at death are shown when information is available. Squares denote male family members and circles denote female family members. (B) Electropherogram of heterozygous *OPTN* c.481G>A (p.Val161Met) point mutation. (C) Conservation of *OPTN* amino acid sequences among different animal species. The valine residue at codon 161 is not necessarily highly conserved among different species (shown in red). Non-conserved amino acids are shown in green.

Table IIIA. Summary of *OPTN* variants identified in FALS patients in previous and present studies.

Studies	Ethnicity	Variant	Number of pedigrees	Status
Maruyama H, et al.[18]	Japanese	exon 5 deletion	4	1 homozygote
		p.Q398X		1 homozygote
		p.E478G		2 heterozygotes
Belzil VV, et al.[19]	European	c.1242 + 1G>A_insA	2	1 heterozygote
		p.A481V		1 heterozygote
Del Bo R, et al.[20]	Italian	p.G23X	2	1 heterozygote
		p.K557T		1 heterozygote
Iida A, et al.[21]	Japanese	p.E478G	1	1 homozygote
Millecamps S, et al.[22]	Caucasian	p.R96L	1	1 heterozygote
Sugihara K, et al.[23]	Caucasian	None	0	
Present study	Japanese	None	0	

mutation identified in an isolated case without any family history, we need to carefully consider various possibilities including the possibilities of causative mutation with reduced penetrance and *de novo* mutation. Another possibility is that the variant might not necessarily be associated with a risk of ALS.

Hexanucleotide repeat expansion within the *C9ORF72* gene has very recently been reported to be frequent as a cause of ALS with wider European ancestry. Our recent study on the same cohort indicated that the frequency of the patients with the hexanucleotide repeat expansions is very low (16), suggesting that the result of our molecular epidemiology study of *OPTN* was not substantially affected by that of *C9ORF72* in our Japanese cohort.

Previous studies showed that the clinical phenotypes of patients with *OPTN* mutations are heterogeneous for both age of onset and disease duration, but are characterized by a relatively slow progression, lower-limb onset, and frequent upper motor neuron signs. The relatively slow progression after the onset and the presence of upper motor neuron signs observed in the patient with the V161M variant are consistent with the previous reports (18–23). However, this patient differed from those in previous reports to the extent that the onset site is the upper extremities. Further accumulation of clinical information is essential to delineate the phenotypic spectrum and to illustrate the genotype-phenotype correlations of ALS with *OPTN* mutations.

Of note, the patient originated from the southernmost part of the Kii Penisula including the Koza River, where the prevalence of ALS has been described to be higher than in other areas of Japan (25). Neither the causes of the high prevalence nor the genetic risk factors common to ALS patients in the region have been elucidated. Mutational analysis of four additional ALS patients residing in the same district (Koza River and its vicinity), however, revealed neither the V161M mutation nor other mutations. V161M does not appear to be very common among the patients with ALS in this district.

Acknowledgements

Table IIIB. Summary of *OPTN* variants identified in SALS patients in previous and present studies.

Studies	Ethnicity	Variant	Number of cases	Status
Maruyama H, et al.[18]	Japanese	p.Q398X	1	1 homozygote
Belzil VV, et al.[19]	European	None	0	
Del Bo R, et al.[20]	Italian	c.552 + 1delG	4	1 heterozygote
		p.T282P		1 heterozygote
		p.Q314L		1 heterozygote
		c.1401 + 4A>G		1 heterozygote
Iida A, et al.[21]	Japanese	p.A93P	2	1 heterozygote
		p.E478G		1 heterozygote
Sugihara K, et al.[23]	Caucasian	None	0	
Present study	Japanese	p.V161M	1	1 heterozygote

566   *H. Naruse et al.*

References

1. Rosen DR, Siddique T, Patterson D, Figlewicz DA, Sapp P, Hentati A, et al. Mutations in Cu/Zn superoxide dismutase gene are associated with familial amyotrophic lateral sclerosis. Nature. 1993;362:59–62.

2. Hadano S, Hand CK, Osuga H, Yanagisawa Y, Otomo A, Devon RS, et al. A gene encoding a putative GTPase regulator is mutated in familial amyotrophic lateral sclerosis 2. Nat Genet. 2001;29:166–73.

3. Yang Y, Hentati A, Deng HX, Dabbagh O, Sasaki T, Hirano M, et al. The gene encoding alsin, a protein with three guanine-nucleotide exchange factor domains, is mutated in a form of recessive amyotrophic lateral sclerosis. Nat Genet. 2001;29:160–5.

4. Puls I, Jonnakuty C, LaMonte BH, Holzbaur EL, Tokito M, Mann E, et al. Mutant dynactin in motor neuron disease. Nat Genet. 2003;33:455–6.

5. Nishimura AL, Mitne-Neto M, Silva HC, Richieri-Costa A, Middleton S, Cascio D, et al. A mutation in the vesicle-trafficking protein VAPB causes late-onset spinal muscular atrophy and amyotrophic lateral sclerosis. Am J Hum Genet. 2004;75:822–31.

6. Parkinson N, Ince PG, Smith MO, Highley R, Skibinski G, Andersen PM, et al. ALS phenotypes with mutations in CHMP2B (charged multivesicular body protein 2B). Neurology. 2006;67:1074–7.

7. Greenway MJ, Andersen PM, Russ C, Ennis S, Cashman S, Donaghy C, et al. ANG mutations segregate with familial and sporadic amyotrophic lateral sclerosis. Nat Genet. 2006;38:411–3.

8. Kabashi E, Valdmanis PN, Dion P, Spiegelman D, McConkey BJ, Vande Velde C, et al. TARDBP mutations in individuals with sporadic and familial amyotrophic lateral sclerosis. Nat Genet. 2008;40:572–4.

9. Kwiatkowski TJ Jr, Bosco DA, Leclerc AL, Tamrazian E, Vanderburg CR, Russ C, et al. Mutations in the FUS/TLS gene on chromosome 16 cause familial amyotrophic lateral sclerosis. Science. 2009;323:1205–8.

10. Vance C, Rogelj B, Hortobágyi T, de Vos KJ, Nishimura AL, Sreedharan J, et al. Mutations in FUS, an RNA processing protein, cause familial amyotrophic lateral sclerosis type 6. Science. 2009;323:1208–11.

11. Dion PA, Daoud H, Rouleau GA. Genetics of motor neuron disorders: new insights into pathogenic mechanisms. Nat Rev Genet. 2009;10:769–82.

12. Alexander MD, Traynor BJ, Miller N, Corr B, Frost E, McQuaid S, et al. 'True' sporadic ALS associated with a novel SOD1 mutation. Ann Neurol. 2002;52:680–3.

13. Chiò A, Calvo A, Moglia C, Ossola I, Brunetti M, Sbaiz L, et al. A de novo missense mutation of the FUS gene in a 'true' sporadic ALS case. Neurobiol Aging. 2011;32: 553.e23–6.

14. DeJesus-Hernandez M, Mackenzie IR, Boeve BF, Boxer AL, Baker M, Rutherford NJ, et al. Expanded GGGGCC hexanucleotide repeat in non-coding region of C9ORF72 causes chromosome 9p-linked FTD and ALS. Neuron. 2011;72:245–56.

15. Renton AE, Majounie E, Waite A, Simon-Sanchez J, Rollinson S, Gibbs JR, et al. A hexanucleotide repeat expansion in C9ORF72 is the cause of chromosome 9p21-linked ALS-FTD. Neuron. 2011;72:257–68.

16. Majounie E, Renton AE, Mok K, Dopper EG, Waite A, Rollinson S, et al. Frequency of the C9orf72 hexanucleotide repeat expansion in patients with amyotrophic lateral sclerosis and frontotemporal dementia: a cross-sectional study. Lancet Neurol. 2012;11:323–30.

17. Deng HX, Chen W, Hong ST, Boycott KM, Gorrie GH, Siddique N, et al. Mutations in UBQLN2 cause dominant X-linked juvenile and adult-onset ALS and ALS/dementia. Nature. 2011;477:211–5.

18. Maruyama H, Morino H, Ito H, Izumi Y, Kato H, Watanabe Y, et al. Mutations of optineurin in amyotrophic lateral sclerosis. Nature. 2010;465:223–6.

19. Belzil VV, Daoud H, Desjarlais A, Bouchard JP, Dupré N, Camu W, et al. Analysis of OPTN as a causative gene for amyotrophic lateral sclerosis. Neurobiol Aging. 2011;32:555.e13–4.

20. Del Bo R, Tiloca C, Pensato V, Corrado L, Ratti A, Ticozzi N, et al. Novel optineurin mutations in patients with familial and sporadic amyotrophic lateral sclerosis. J Neurol Neurosurg Psychiatry. 2011;82:1239–43.

21. Iida A, Hosono N, Sano M, Kamei T, Oshima S, Tokuda T, et al. Optineurin mutations in Japanese amyotrophic lateral sclerosis. J Neurol Neurosurg Psychiatry. 2012;83:233–5.

22. Millecamps S, Boillée S, Chabrol E, Camu W, Cazeneuve C, Salachas F, et al. Screening of OPTN in French familial amyotrophic lateral sclerosis. Neurobiol Aging. 2011;32: 557.e11–3.

23. Sugihara K, Maruyama H, Kamada M, Morino H, Kawakami H. Screening for OPTN mutations in amyotrophic lateral sclerosis in a mainly Caucasian population. Neurobiol Aging. 2011;32:1923.e9–10.

24. Takahashi Y, Seki N, Ishiura H, Mitsui J, Matsukawa T, Kishino A, et al. Development of a high-throughput microarray-based resequencing system for neurological disorders and its application to molecular genetics of amyotrophic lateral sclerosis. Arch Neurol. 2008;65:1326–32.

25. Yoshida S, Uebayashi Y, Kihira T, Kohmoto J, Wakayama I, Taguchi S, et al. Epidemiology of motor neuron disease in the Kii Peninsula of Japan, 1989–1993: active or disappearing focus? J Neurol Sci. 1998;155:146–55.

ORIGINAL ARTICLE

α-Synuclein Pathology in the Amyotrophic Lateral Sclerosis/ Parkinsonism Dementia Complex in the Kii Peninsula, Japan

Yasumasa Kokubo, MD, PhD, Akira Taniguchi, MD, Masato Hasegawa, PhD, Yuma Hayakawa, Satoru Morimoto, MD, Misao Yoneda, PhD, Yoshihumi Hirokawa, MD, PhD, Taizo Shiraishi, MD, PhD, Yuko Saito, MD, PhD, Shigeo Murayama, MD, PhD, and Shigeki Kuzuhara, MD, PhD

Abstract

α-Synuclein pathology was examined in the brains and spinal cords of 10 patients with amyotrophic lateral sclerosis (ALS)/parkinsonism-dementia complex (PDC) in the Kii Peninsula, Japan. Various types of phosphorylated α-synuclein–positive structures including neuronal cytoplasmic inclusions, dystrophic neurites, and glial cytoplasmic inclusions were found in all ALS/PDC cases. There were phosphorylated α-synuclein–positive neurons in 8 cases (80%), and the amygdala was most severely affected. Phosphorylated α-synuclein was distributed mainly in the limbic system and brainstem; tau pathology was more prevalent than α-synuclein pathology in most affected areas. In the substantia nigra, periaqueductal gray, locus coeruleus, raphe nuclei, dorsal nucleus of the vagus nerve, hypoglossal nucleus or ventral horn, and intermediolateral nucleus of the spinal cord, α-synuclein pathology was more predominant than tau pathology in only 1 or 2 patients. Phosphorylated α-synuclein– positive structures were not found in the molecular layer of the cerebellum. Phosphorylated α-synuclein frequently colocalized with tau in neuron cell bodies, neurites, and glia. Immunoblots of sarkosyl-insoluble fractions extracted from the brain of 1 patient showed a triplet of α-synuclein–immunoreactive bands that were ubiquitinated. These results suggest that interaction between tau and α-synuclein be involved in the pathogenesis of Kii ALS/PDC.

Key Words: α-Synuclein, Amyotrophic lateral sclerosis, Guam, Kii Peninsula, Parkinsonism-dementia complex, Tau.

INTRODUCTION

Amyotrophic lateral sclerosis/parkinsonism-dementia complex (ALS/PDC) is a neurodegenerative disease endemic to Guam and the Kii Peninsula of Japan (1–3). The clinical picture of ALS/PDC is a unique combination of parkinsonism, dementia, and symptoms of upper and lower motor neuronal dysfunction. Neuropathologic findings of ALS/PDC include numerous neurofibrillary tangles (NFTs) associated with nerve cell loss in the cerebral cortex and brainstem in addition to ALS pathology. Our investigation of the topographical distribution of NFTs suggested that ALS and PDC in the Kii Peninsula comprise part of a spectrum of tauopathies (4).

α-Synuclein is a presynaptic protein. Phosphorylated α-synuclein is the main component of Lewy bodies (LBs) that are characteristic of Parkinson disease and dementia with LBs (DLB), and of the glial cytoplasmic inclusions found in multiple system atrophy (5, 6). In Guamanian patients with PDC, α-synuclein–positive structures have been detected in the amygdala in approximately 40% of cases (7, 8) and in the cerebellum in more than 60% of cases (9). In this report, we examined phosphorylated α-synuclein immunoreactivity in the brains and spinal cords from 10 patients with ALS/PDC from the Kii Peninsula (Kii ALS/PDC) and analyzed biochemical aspects of α-synuclein from 1 patient.

MATERIALS AND METHODS

Cases

We examined 10 patients with neuropathologically verified Kii ALS/PDC (mean age, 69.1 years; range, 60–77 years). Demographic features and clinical manifestations are listed in Table 1. This study was approved by the ethics committee of Mie University Graduate School of Medicine. Informed consent was obtained from the patients or their families.

Neuropathology and Immunohistochemistry

The brains and spinal cords were fixed in formalin solution for 2 to 3 weeks. The brains were sliced into coronal sections and the spinal cords were sliced axially. Paraffin-embedded samples were cut into 9-μm-thick sections for hematoxylin and eosin, Klüver-Barrera, and Gallyas-Braak staining. All histologic samples showed numerous NFTs

TABLE 1. Clinical Data

Case No.	Age, y	Sex	Duration of Illness, y	Phenotype		
				A	P	D
1	70	F	13	+	−	−
2	63	F	5	+	−	−
3	66	F	3	+	−	−
4	65	M	3	+	−	+
5	77	M	7	+	−	+
6	70	F	8	+	+	+
7	60	F	7	+	+	+
8	76	F	6	+	+	+
9	70	F	14	−	+	+
10	74	M	6	−	+	+

A, Amyotrophic lateral sclerosis; P, parkinsonism, D, dementia; F, female; M, male; −, absent; +, present.

without senile plaques. Nerve cell loss was chiefly in the temporal cortex, frontal cortex, and the nuclei of the brain-stem. Loss of anterior horn cells and degeneration of pyramidal tracts were common features.

Six-micrometer-thick sections were prepared for immunohistochemical studies. Immunostaining was performed using the avidin-biotin-peroxidase complex (ABC) method with a Vectastain ABC kit (Vector Laboratories, Burlingame, CA). The antibodies used and their dilutions were as follows: anti-phosphorylated α-synuclein antibody specifically recognizes phosphorylation at Ser-129 (PSer129, 1:5000; monoclonal; Wako, Osaka, Japan) and anti–phosphorylated tau antibody (AT8, 1:100; monoclonal; Innogenetics, Ghent, Belgium). Regions selected for evaluation are shown in Table 2. To evaluate the phosphorylated α-synuclein–positive structures and phosphorylated tau-positive structures, scores ranging from (−) to (+++) were assigned according to the number of structures in the area of maximum density. Phosphorylated α-synuclein–positive and phosphorylated tau-positive neurons were counted in 100× microscopic fields. Densities of phosphorylated α-synuclein–positive were scored as follows: −, 0; ±, 1; +, 2 to 5; ++, 6 to 10; +++, more than 10/field. Densities of phosphorylated tau-positive neurons were scored as follows: −, 0; +, 1 to 10; ++, 11 to 20; +++, more than 20/field. Colocalization of phosphorylated α-synuclein and phosphorylated tau was determined in sections double-labeled with PSer129 antibody and AT8 antibody using immunofluorescent substrate (Alexa Fluor 488 and 546; Life Technologies, Carlsbad, CA).

Western Blot

Sarkosyl-insoluble α-synuclein was extracted from the hippocampus of case 10. Sarkosyl-insoluble α-synuclein was prepared as previously described (10, 11) with slight modifications. Briefly, frozen brain tissue samples were homogenized in a 20-fold volume of buffer A (10 mmol/L Tris, pH 7.5, 1 mmol/L EGTA, 1 mmol/L dithiothreitol, 10% sucrose) containing 1% Triton X-100, incubated for 30 minutes at 37°C and spun at 100,000 × g for 30 minutes at 25°C. The resultant pellets were subsequently homogenized in buffer A containing 1% sarkosyl, incubated at 37°C for 30 minutes, and centrifuged 100,000 × g for 30 minutes. The sarkosyl-

insoluble pellet was homogenized in 4 volumes of buffer A containing 1% CHAPS and spun at 100,000 × g for 20 minutes. The pellet was sonicated in 1 volume of 8 mol/L urea and spun at 100,000 × g for 20 minutes. The supernatant was mixed with an equal volume of 2× SDS sample buffer and treated at 100°C for 3 minutes. Aliquots of the samples were separated on a 10% or 15% sodium dodecyl sulfate (SDS)–polyacrylamide gel and transferred to a polyvinylidene difluoride membrane. The membrane was then probed with PSer129 (1:2000) and phosphorylation-independent anti–α-synuclein antibody (Syn 102: mouse monoclonal antibody, epitope location on α-synuclein residues 131–140) (12).

In vitro ubiquitination of α-synuclein was performed as previously described (12) with minor modifications. Briefly, 20 μg of human recombinant α-synuclein and 2 μg of ubiquitin (derived from bovine blood cells) or methylated ubiquitin were incubated with an ubiquitin ligase fraction (Fraction II) from rabbit reticulocytes at 37°C for 2 hours in a buffer containing 50 mmol/L Tris-HCl (pH 9.0), 2 mmol/L ATP, 5 mmol/L MgCl₂, and 1 mmol/L dithiothreitol. The conjugation reaction was stopped by boiling the samples in an equal volume of SDS sample buffer followed by separation of the components by SDS–polyacrylamide gel electrophoresis. To examine the ubiquitinated state of α-synuclein, we compared the mobilities of α-synuclein derived from Kii ALS/PDC, ubiquitinated, and unubiquitinated recombinant α-synuclein by SDS–polyacrylamide gel electrophoresis using anti-ubiquitin monoclonal antibody 1510 (anti-Ub 1510) (12). Ubiquitinated and unubiquitinated recombinant α-synuclein were identified by labeling with PSer129 and Syn102.

RESULTS

A representative image of a neuron with LBs and adjacent neurons with NFTs is shown in Figure 1A. Various types of phosphorylated α-synuclein–positive structures, including neuronal cytoplasmic inclusions and LBs (Fig. 1B), Lewy neurites (Fig. 1C), and glial cytoplasmic inclusions (Fig. 1D), were found in all ALS/PDC cases. There were no neuronal intranuclear inclusions. Phosphorylated α-synuclein–positive neurons were found in 8 (80%) of the 10 cases. Phosphorylated α-synuclein–positive neurons were

626

TABLE 2. Topographical Distribution of α-Synuclein–Positive Neurons and Tau-Positive Neurons

		Case 1	Case 2	Case 3	Case 4	Case 5	Case 6	Case 7	Case 8	Case 9	Case 10
Diagnosis:		ALS	ALS	ALS	ALS With D	ALS With D	PDC	PDC	PDC	PDC	PDC
Sex		F	F	F	M	M	F	F	F	F	M
Age, y		70	63	66	65	77	70	60	76	70	75
Frontal cortex BA8/9	Tau	−	+	+	++	NA	++	+	++	+	−
	αS	−	−	NA	−	−	−	−	−	−	−
Cingulate gyrus BA24	Tau	−	+	NA	+	NA	NA	−	+	++	−
	αS	−	−	NA	−	−	−	−	−	−	−
Insula	Tau	+	++	+	++	+	++	++	+	++	+
	αS	−	−	NA	−	−	−	−	−	−	+
Parietal cortex BA40	Tau	NA	NA	NA	+	NA	NA	NA	+	−	+
	αS	−	−	NA	−	NA	NA	NA	NA	−	±
Temporal cortex BA21	Tau	+	+++	+	+	+++	+++	++	++	++	+
	αS	−	−	−	−	−	−	−	±	−	+
Hippocampus (Ammon horn)	Tau	+++	+++	+	+++	+++	+++	+++	+++	+++	+++
	αS	−	−	−	−	−	−	++	+	−	++
Meynert nucleus	Tau	+	+	NA	++	++	++	+++	NA	+	+
	αS	−	−	NA	−	−	−	+++	NA	−	−
Caudate nucleus	Tau	−	+	NA	+	+	NA	±	+	+	−
	αS	−	−	NA	−	−	−	+	−	+	−
Putamen	Tau	+	++	NA	+	+	NA	±	+	+	+
	αS	−	−	NA	−	−	−	+	−	−	−
Pallidum	Tau	−	+	NA	+	+	NA	±	NA	+	+
	αS	−	−	NA	−	−	−	+	NA	−	−
Transentorhinal cortex BA28	Tau	++	+++	+	++	++	+++	+++	+++	++	+++
	αS	−	−	−	−	−	−	+	++	−	±
Motor cortex	Tau	NA	+	NA	+	+	++	+	+	++	NA
	αS	NA	NA	NA	−	−	−	−	−	−	−
Thalamus	Tau	−	+	+	+	−	NA	++	+	++	+
	αS	−	NA	NA	−	−	NA	−	NA	−	−
Subthalamic nucleus	Tau	−	+	NA	+	NA	NA	NA	+	+	+
	αS	−	NA	NA	−	NA	NA	NA	NA	±	±
Amygdala	Tau	+++	+++	+++	+++	+++	++	+++	++	+++	+++
	αS	−	−	−	+	+	+	++	+	±	+++
Parahippocampus	Tau	+++	+++	+	++	+++	+++	+++	+++	+++	+++
	αS	−	−	−	−	−	−	++	+	−	+++
Cerebellum Molecular layer	Tau	−	−	−	−	−	−	+	−	−	−
	αS	−	−	−	−	−	−	−	−	−	−
Dentate nucleus	Tau	−	+	−	+	+	+	++	+	+++	+
	αS	−	−	−	+	−	−	−	+	−	−
White matter	Tau	−	−	−	−	−	+	−	−	+	−
	αS	−	−	−	−	−	−	−	±	−	−
Midbrain Substantia nigra	Tau	−	+	+	+	+	++	+	+++	+++	++
	αS	++	−	−	+	−	−	++	+	−	++
Periaqueductal gray	Tau	+	+++	+++	+++	+	+	++	+++	+++	+++
	αS	+	−	−	+	−	−	+++	++	−	++
Pons Locus coeruleus	Tau	+	++	+	+	+	+	+	+++	+++	+++
	αS	+++	−	−	+++	−	−	−	+++	−	+++
Raphe nuclei	Tau	+	+	+	+	+	+	+	+	+++	+++
	αS	−	−	−	+	−	−	−	+++	−	++
Pontine nucleus	Tau	−	−	−	−	−	−	−	+	+++	−
	αS	−	−	−	−	−	−	−	−	−	−

(Continued on next page)

TABLE 2. *(Continued)*

			Case 1	Case 2	Case 3	Case 4	Case 5	Case 6	Case 7	Case 8	Case 9	Case 10
Diagnosis:			ALS	ALS	ALS	ALS With D	ALS With D	PDC	PDC	PDC	PDC	PDC
Sex			F	F	F	M	M	F	F	F	F	M
Age, y		70	63	66	65	77	70	60	76	70	75	
Medulla	Dorsal nucleus of vagus nerve	Tau	+	+	−	−	−	+	−	−	−	+
		αS	+	−	−	+++	−	−	−	−	−	+++
	Hypoglossal nucleus	Tau	+	±	−	−	−	+	+	−	+	−
		αS	−	−	−	−	−	−	−	−	−	+
	Inferior olivary nucleus	Tau	−	−	−	−	−	+	+	−	+	++
		αS	−	−	−	−	−	−	−	−	−	+
spinal cord	Ventral horn	Tau	−	−	−	NA	−	−	+	+	++	+
		αS	−	−	−	NA	−	−	−	++	−	+
	Intermediolateral nucleus	Tau	−	−	+	NA	−	−	+	+	+	−
		αS	±	−	−	NA	−	−	±	−	−	+++

α-Synuclein (αS)–positive neurons were counted in microscope fields at a magnification of 100× and the density of α-synuclein positive neurons was scored as follows: −, 0; ±, 1; +, 2 to 5; ++, 6 to 10; +++, more than 10. The density of tau-positive neurons was scored at a magnification of 100× as follows: to , 0; +, 1 to 10; ++, 11 to 20; +++, more than 20.

mainly detected in the amygdala (70%); substantia nigra, periaqueductal gray (50%); locus coeruleus (40%); and hippocampus, transentorhinal cortex, parahippocampus, raphe nucleus, dorsal vagal nucleus, and intermediolateral nucleus of the spinal cord (30%) (Table 2). There were no phosphorylated α-synuclein–positive structures in the molecular layer of the cerebellum in any of the 10 cases. Tau-positive

neurons were abundant in most areas examined. Phosphorylated α-synuclein–positive neurons outnumbered tau-positive neurons in the substantia nigra, locus coeruleus, and dorsal nucleus of the vagus nerve in a few patients, and periaqueductal gray, raphe nucleus, spinal ventral horn, and spinal intermediolateral nucleus in only 1 or 2 patients (Table 2). Semiquantitative evaluation suggested that the densities of
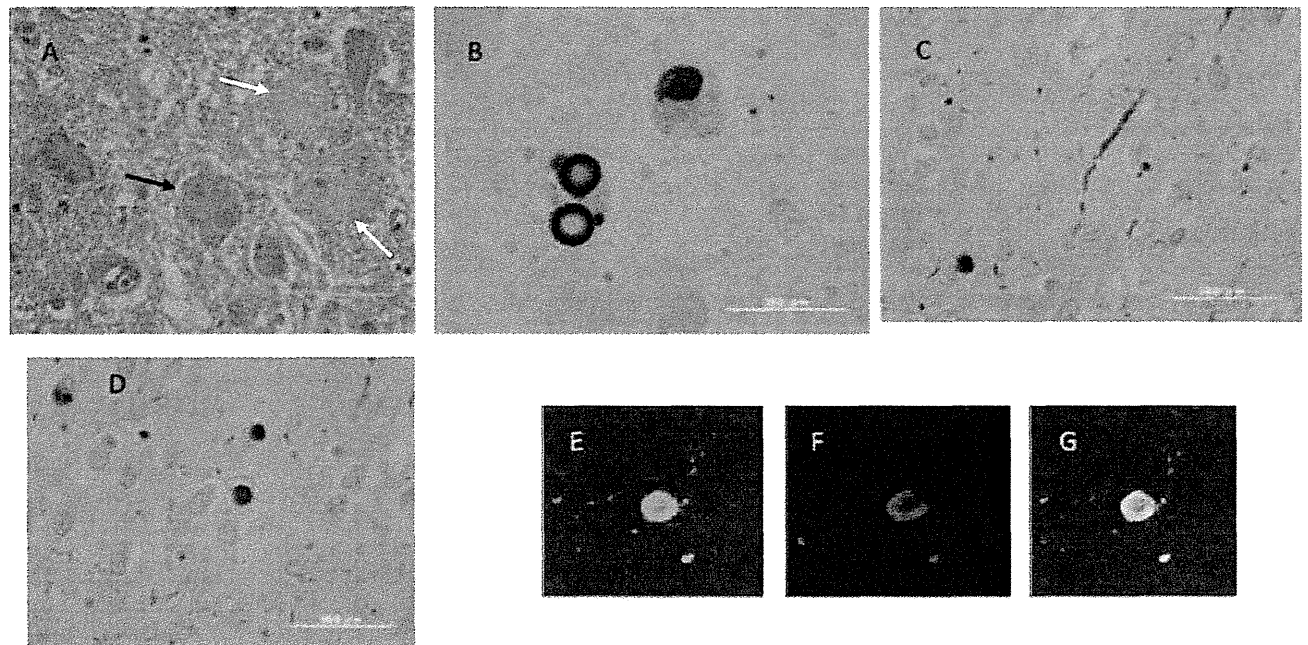

FIGURE 1. Hematoxylin and eosin staining, immunostaining using an antibody against phosphorylated α-synuclein (PSer129), and double immunofluorescence with PSer129 and anti-phosphorylated tau (AT8) antibodies. **(A)** Lewy bodies (LBs) (black arrow) and neurofibrillary tangles (NFTs) (yellow arrows) in the locus coeruleus (hematoxylin and eosin stain). **(B)** LBs and cytoplasmic round inclusion in the locus coeruleus (PSer129). **(C)** Lewy neurites in the amygdala (PSer129). **(D)** Glial cytoplasmic inclusion in the amygdala (PSer129). **(E–G)** Double immunofluorescence labeling showing the coexistence of α-synuclein (PSer129, Alexa 488: green) **(E)**, tau (AT8, Alexa 546: red) **(F)**, and their merged image **(G)**.

628   © *2012 American Association of Neuropathologists, Inc.*
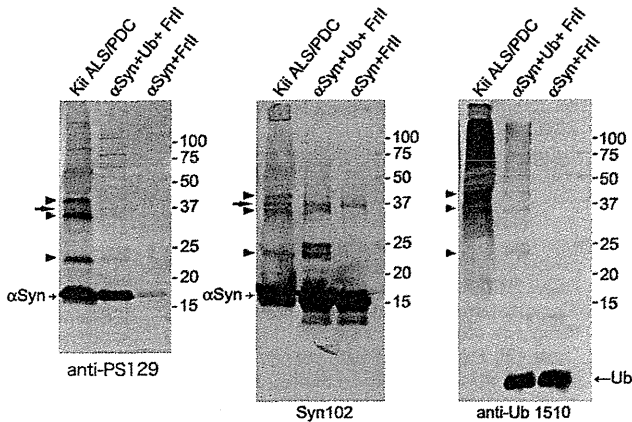
FIGURE 2. Sarkosyl-insoluble fractions from case 10 with Kii amyotrophic lateral sclerosis/parkinsonism dementia complex (ALS/PDC), ubiquitinated recombinant α-synuclein (αSyn + Ub + Frll), and nonubiquitinated recombinant α-synuclein (αSyn + Frll). Samples were immunoblotted with a phosphorylation-dependent anti–α-synuclein antibody (anti-PSer129) (PS129), a phosphorylation-independent anti–α-synuclein antibody (Syn 102), and an anti-ubiquitin (Ub) antibody (anti-Ub 1510). Note that 24-, 32-, and 40-kDa bands are detected in the Kii ALS/PDC brain and αSyn + Ub + Frll with anti-PSer129, Syn 102, and anti-Ub 1510 (arrowheads). Arrow indicates an α-synuclein dimer, which was also detected in αSyn + Frll.

phosphorylated α-synuclein–positive neurons were not related to age or duration of illness but to the densities of tau-positive neurons. Colocalization of phosphorylated α- synuclein and phophorylated tau was observed in many neuronal cytoplasmic inclusions and neuropil threads in the amygdala, substantia nigra, periaqueductal gray, locus coeruleus (Figs. 1E–G), hippocampus, transentorhinal cortex, and parahippocampus.

Immunoblots of sarkosyl-insoluble fractions extracted from the brain of a Kii ALS/PDC patient showed a few α-synuclein–immunoreactive bands. The major immunoreactive band with an apparent molecular mass of 17 kDa and minor 24-, 32-, and 40-kDa bands migrating at a higher molecular mass range on the Tris–glycine gel system were immunoreactive with PSer129 and Syn102. The higher molecular mass of phosphorylated α-synuclein–related polypeptides suggested ubiquitination compared with recombinant α-synuclein, which was incubated with the ubiquitin ligase fraction with or without ubiquitin (Fig. 2), as previously reported in other synucleinopathies (12).

DISCUSSION

α-Synuclein–positive pathology has been identified in a variety of disorders with extensive tau pathology including sporadic Alzheimer disease (13, 14), familial Alzheimer disease (15), DLB (16), familial DLB (17), familial Parkinson disease associated with the α-synuclein A53T mutation (18), Down syndrome (19), neurodegeneration with brain iron accumulation (20–22), and Guam PDC (7–9). Colocalization of tau and α-synuclein was variable in these diseases. For example, extensive colocalization of tau and α-synuclein was reported in DLB (16)

and familial DLB (17); the co-occurrence of tau and α-synuclein was variable in Guam PDC (7, 8).

In the present study, the frequency, distribution, and morphology of α-synuclein deposits are described in the brains and spinal cords of patients with Kii ALS/PDC for the first time. α-Synuclein deposits were observed mainly in the limbic system and brainstem; α-synuclein was phosphorylated and ubiquitinated. Tau-positive neurons were more abundant than α-synuclein–positive neurons in most areas examined, and there was extensive colocalization of tau and α-synuclein.

Although Kii ALS/PDC and Guam ALS/PDC share a number of clinical and neuropathologic features, it remains unclear whether they are identical. Yamazaki et al (7) examined α-synuclein–positive intraneuronal inclusions in the motor cortex, medial temporal lobe, and brainstem of 13 patients with Guam PDC using antibodies against non-phosphorylated α-synuclein; they found that 7 (54%) of 13 PDC patients showed α-synuclein–positive inclusions in at least 1 region of the brain. The authors concluded that the amygdala was most affected by α-synuclein pathology, in which α-synuclein was frequently colocalized with tau. Forman et al (8) reported that α-synuclein pathology of the amygdala in Guam ALS/PDC was present in 37% of 19 patients with PDC, but absent in patients with ALS, preclinical PDC, early PDC/ALS, clinical (pathology pending) PDC, PDC/ALS, and control Chamorro patients. The α-synuclein aggregates rarely colocalized within neurons harboring NFTs. On the basis of these findings, the authors suggested a possible interaction between tau and α-synuclein and tau deposits preceding α-synuclein deposits. Sebeo et al (9) reported that numerous α-synuclein–immunoreactive spherical structures in the molecular layer of the cerebellum were observed in 63.6% of Guam PDC patients. These structures were seen exclusively in patients showing α-synuclein pathology in the amygdala, and were much more pronounced in the hemisphere than in the vermis and were associated with Purkinje cells and Bergmann glia cells.

We found that in Kii ALS/PDC, α-synuclein pathology in the amygdala was absent in patients with ALS but was present in ALS patients with dementia and PDC. These results suggest that the α-synuclein pathology in the amygdala may have been induced by tau deposition and may be related to dementia in ALS/PDC. Because α-synuclein inclusions are not found in every brain with other tauopathies, tau in ALS/PDC cases might accelerate α-synuclein aggregation. The combination of misfolded α-synuclein and tau that occurs in ALS/PDC might promote cytotoxic protofibrils and accelerate protein deposits (23). We carefully searched the cerebellum of Kii ALS/PDC patients for similar α-synuclein–positive structures in the molecular layer but failed to find α-synuclein–positive pathology. In general, neuronal cell loss and tau deposits in the molecular layer are exceptional in Kii ALS/PDC. The cause of this discrepancy in α-synuclein pathology in the cerebellum between Guam ALS/PDC and Kii ALS/PDC might be clarified by using the same antibody and identical staining protocols in further studies.

In summary, α-synuclein–positive structures were common in both ALS and PDC and were mainly distributed